Cellular and Molecular Life Sciences (2021) 78:963–983
https://doi.org/10.1007/s00018-020-03546-3

ORIGINAL ARTICLE

Studies of *ApoD*$^{-/-}$ and *ApoD*$^{-/-}$*ApoE*$^{-/-}$ mice uncover the APOD significance for retinal metabolism, function, and status of chorioretinal blood vessels

Nicole El-Darzi[1] · Natalia Mast[1] · Alexey M. Petrov[1] · Tung Dao[1] · Artem A. Astafev[1] · Aicha Saadane[1] · Erin Prendergast[2] · Emmy Schwarz[2] · Ilya Bederman[2] · Irina A. Pikuleva[1]

Received: 29 January 2020 / Revised: 15 April 2020 / Accepted: 7 May 2020 / Published online: 21 May 2020

Abstract

Apolipoprotein D (APOD) is an atypical apolipoprotein with unknown significance for retinal structure and function. Conversely, apolipoprotein E (APOE) is a typical apolipoprotein with established roles in retinal cholesterol transport. Herein, we immunolocalized APOD to the photoreceptor inner segments and conducted ophthalmic characterizations of *ApoD*$^{-/-}$ and *ApoD*$^{-/-}$*ApoE*$^{-/-}$ mice. *ApoD*$^{-/-}$ mice had normal levels of retinal sterols but changes in the chorioretinal blood vessels and impaired retinal function. The whole-body glucose disposal was impaired in this genotype but the retinal glucose metabolism was unchanged. *ApoD*$^{-/-}$*ApoE*$^{-/-}$ mice had altered sterol profile in the retina but apparently normal chorioretinal vasculature and function. The whole-body glucose disposal and retinal glucose utilization were enhanced in this genotype. OB-Rb, both leptin and APOD receptor, was found to be expressed in the photoreceptor inner segments and was at increased abundance in the *ApoD*$^{-/-}$ and *ApoD*$^{-/-}$*ApoE*$^{-/-}$ retinas. Retinal levels of *Glut4* and *Cd36*, the glucose transporter and scavenger receptor, respectively, were increased as well, thus linking APOD to retinal glucose and fatty acid metabolism and suggesting the APOD-OB-Rb-GLUT4/CD36 axis. In vivo isotopic labeling, transmission electron microscopy, and retinal proteomics provided additional insights into the mechanism underlying the retinal phenotypes of *ApoD*$^{-/-}$ and *ApoD*$^{-/-}$*ApoE*$^{-/-}$ mice. Collectively, our data suggest that the APOD roles in the retina are context specific and could determine retinal glucose fluxes into different pathways. APOD and APOE do not play redundant, complementary or opposing roles in the retina, rather their interplay is more complex and reflects retinal responses elicited by lack of these apolipoproteins.

Keywords Cholesterol · Glucose · Fatty acids · Leptin receptor · Apolipoprotein · Isotopic labeling

Abbreviations

APOE	Apolipoprotein E
APOD	Apolipoprotein D
AQ4	Aquaporin 4
ERG	Electroretinographic recordings
FA	Fluorescein angiography
FI	Fundus imaging
GC–MS	Gas chromatography–mass spectroscopy
HFHS	High-fat high-sugar diet
IS	Photoreceptor inner segments
NGS	Normal goat serum
PBS	Phosphate buffer saline
RPE	Retinal pigment epithelium
SD-OCT	Spectral-domain optical coherence tomography
TCA	The tricarboxylic acid cycle
TEM	Transmission electron microscopy

Electronic supplementary material The online version of this article (https://doi.org/10.1007/s00018-020-03546-3) contains supplementary material, which is available to authorized users.

✉ Irina A. Pikuleva
iap8@case.edu

[1] Department of Ophthalmology and Visual Sciences, Case Western Reserve University, Cleveland, OH, USA

[2] Department of Genetics and Genome Sciences, Case Western Reserve University, Cleveland, OH, USA

Introduction

The retina is a multi-layered light-sensitive tissue lining the back of the eye. The retina is rich in cholesterol, whose levels represent a balance between the pathways of cholesterol input and output [1, 2]. The apolipoprotein-containing particles are important contributors to cholesterol homeostasis

in the retina as they traffic in the intraretinal space and either deliver cholesterol to different retinal cells or remove cellular cholesterol excess when it is effluxed from cells [3, 4]. Apolipoprotein E (APOE) is a typical apolipoprotein [5] and one of the most abundant apolipoproteins in the retina [6]. The canonical APOE roles in the CNS are to transport cholesterol and other lipids and serve as a recognition ligand for the receptors that interact with the APOE-containing lipoprotein particles [7]. In addition, APOE was found to be involved in other important processes such as immunomodulation, synaptic plasticity, signal transduction, proteostasis and other [5, 8–10]. The APOE isoform ε4 is a risk factor for developing Alzheimer's disease but is protective against age-related macular degeneration, a blinding retinal disease. Conversely, the APOE ε2 isoform decreases and increases risks for Alzheimer's disease and age-related macular degeneration, respectively [11–16]. Remarkably, total APOE absence does not seem to affect neurocognitive and retinal functions in humans [17], possibly because of the compensatory responses and/or the fact that there are other apolipoproteins in the brain and retina [6, 18] whose functions could be redundant.

Apolipoprotein D (APOD) is an atypical apolipoprotein, because it does not share sequence similarity with other apolipoproteins [19] and is poorly expressed in the liver and intestine, the major expression sites for most apolipoproteins. Instead, APOD is expressed in many extrahepatic tissues (e.g., brain, testes, adrenal glands, spleen, and kidneys [20–22]), where it could be found in the cytoplasm, outer cell membrane, or perinuclear membrane area [23, 24]. APOD is a lipocalin and as such has a ligand-binding cup, which can accommodate different hydrophobic molecules (e.g., arachidonic acid, pregnenolone, progesterone, and cholesterol [22, 25]). This structural feature renders APOD a tissue-specific hydrophobic molecule carrier [26]. In addition, APOD was found to interact with the membrane receptors BASI (basigin, Suppl. Text T1), OB-Rb (the long form of the leptin receptor), and SR-B1 (scavenger receptor class B member 1) [27–29]), and thereby participate in different signaling pathways (e.g., MAPK/FOS and JAK2/STAT3 [30–34]). Human but not mouse APOD has a free cysteine residue on a surface loop, which mediates APOD dimerization or binding to other cysteine-containing proteins (e.g., APOAII on HDL and APOB on LDL or VLDL [35]). APOD also has an N-terminal 3_{10}-α-helix found in proteins associated with endosomal trafficking [23].

APOD was shown to be both neuro- and cardioprotective and play antioxidant, anti-inflammatory, and stress resistance roles (reviewed in [25, 36, 37]). The APOD levels are altered in such neurologic conditions as Alzheimer's and Parkinson diseases, schizophrenia, and stroke (reviewed in [25]) as well as in several types of cancer [23, 38–42], disorders of lipid metabolism (reviewed in [43]), and type 2 diabetes [44]. The APOD polymorphisms were reported to be associated with obesity and hyperinsulinemia [45], type 2 diabetes [46], cardiovascular risk [47], and Alzheimer's disease [48–50]. Notably, APOD is the most upregulated gene in the aging human brain [51], and this upregulation is conserved among humans, macaques, and mice [51–53]. Nevertheless, despite numerous studies, the principal physiological roles of APOD have not yet been established.

In the CNS, the APOE and APOD expression may be coordinated [54–57]. The APOD levels were shown to be increased in the brain of *ApoE*$^{-/-}$ mice [54, 55] and were suggested to underlie the unaltered levels of the whole brain cholesterol [55]. Moreover, an inverse correlation was found between the *ApoD* and *ApoE* expression in most regions of mouse brain [56]. Similarly, in fly glial cells, loss of the *ApoD* analogs *Glaz* and *Nlaz* was compensated by human APOE expression [57]. In human hepatic and glioblastoma cell lines, the APOE ε3 and ε4 were even shown to be present in the nucleus and bind to the *ApoD* promoter, thus repressing its activity [56]. Yet there is an overlap in the transcription factors (liver X receptors) that regulate the *ApoE* and *ApoD* expression [58]. Also, there are reports on simultaneous increases in the levels of *ApoE* and *ApoD* or their protein products under different trauma conditions (a denervating crush injury [59] and limbic status epilepticus [60]) or in cell cultures modeling the regeneration of damaged peripheral neurons [61] and under growth arrest [62].

Very little is currently known about the role of APOD in the retina. One study found that *ApoD* was downregulated in a mouse model of the Norrie disease, a neurologic disorder [63]. Another study showed that *ApoD* was upregulated in normal mice in response to high-fat high-cholesterol diet or treatment with the liver X receptor agonist TO901317 [64]. Accordingly, to gain insight into retinal significance of APOD and potential retinal APOD-APOE link, we characterized *ApoD*$^{-/-}$ mice and also generated and characterized *ApoD*$^{-/-}$*ApoE*$^{-/-}$ mice.

Materials and methods

Animals

Female and male mice 6–12 months of age were used. C57BL/6J, *ApoD*$^{-/-}$, and *ApoE*$^{-/-}$ mice on the C57BL/6J background were from the Jackson Laboratory (000664, 018292, and 002052, respectively). *ApoD*$^{-/-}$*ApoE*$^{-/-}$ mice were generated by crossing *ApoD*$^{-/-}$ and *ApoE*$^{-/-}$ mice. All animals were free of the *Crbl*^{rd8} mutation. Mice were maintained on a standard 12-h light (~ 10 lx)-dark cycle and were provided regular rodent chow and water ad libitum. For dietary treatments, the Western diet (Research Diets Inc., D12079B, containing 0.3% cholesterol and 0.21% milk fat)

and high-fat high-sugar diet (HFHS diet, Research Diets Inc., D12451, containing 17% sucrose 18% lard, and 2.5% soybean oil) were used. The latter diet was supplemented with 20% fructose in drinking water. Animal were put on these diets for 5 and 3 months, respectively, after weaning, approximately, at 1 month of age. All animal experiments were approved by Case Western Reserve University's IACUC and conformed to recommendations of the American Veterinary Association Panel on Euthanasia.

In vivo characterizations

Mice were anesthetized via intraperitoneal injection of 80 mg/kg ketamine and 15 mg/kg xylazine (Patterson Veterinary, 07-890-85598 and 07-808-1947, respectively) in sterile distilled water. Ultra-high resolution spectral-domain optical coherence tomography (SD-OCT), fluorescein angiography (FA), and electroretinographic recordings (ERG) were carried out as described [65, 66]. An 840HHP SD-OCT system (Bioptigen), a scanning laser ophthalmoscope (Spectralis HRA + OCT, Heidelberg Engineering), and an Electrophysiological System UTAS E-3000 (LKC Technologies Inc.) were used. Images for FA were acquired after a bolus (0.1 ml) intraperitoneal injection of 1.0% sodium fluorescein (Akorn) in phosphate buffer saline (PBS). Fundus imaging (FI) was carried out using iVivo Funduscope (OcuScience-Xenotec, Inc.) according to the manufacturer's instructions.

Histochemistry and immunohistochemistry

Stains for unesterified (free) cholesterol with filipin and for albumin were as described [67–69]. For the APOD immunolocalizations, mice underwent cardiac perfusion with 30 ml of PBS, pH 7.4, and then with 20 ml of 4% paraformaldehyde in 0.1 M potassium phosphate buffer, pH 7.2. Sections were prepared as described [66], deparaffinized, and the antigen retrieval was performed at 95 °C for 30 min in 10 mM Tris-HCl buffer, pH 9.0, containing 1 mM EDTA and 0.05% Tween 20. Subsequent section processing was as described [66]. The blocking buffer was PBS containing 5% normal goat serum (NGS, Life Technologies, PCN5000) and 0.05% Tween 20. The primary antibody was rabbit anti-APOD (LifeSpan, LS-82158), and the secondary antibody was goat anti-rabbit Alexa Fluor 647 (Jackson ImmunoResearch, 111-605-144) diluted 1:50 and 1:200, respectively, with PBS containing 5% NGS and 0.05% Tween 20. The washing buffer was PBS containing 0.05% Tween 20. For the OB-Rb immunolocalization, the cardiac perfusions were not performed, and the antigen retrieval was at 90 °C for 30 min in 10 mM citrate buffer, pH 6.0, containing 0.05% Tween 20. The blocking buffer was PBS containing 10% NGS, 1% BSA, and 0.1% Triton X-100. The primary antibody was rabbit anti-OB-Rb (Invitrogen, PA1-053), and the secondary antibody was goat anti-rabbit Alexa Fluor 647 diluted 1:600 and 1:200, respectively, with PBS containing 10% NGS and 1% BSA. The washing buffer was PBS containing 0.05% Tween 20. Sections were covered either with ProLong Gold antifade reagent with DAPI (Molecular Probes, P36935) or DAPI Fluoromount-G (SouthernBiotech, 0100-20) and protected with a glass coverslip. Filipin and anti-APOD stainings were imaged on an inverted Leica microscope (Leica Microsystems, DMI6000B), whereas the anti-OB-Rb and anti-albumin stainings were imaged on an Olympus Fluoview FV1200 Laser Scanning Confocal Microscope.

Retina isolation and sterol content in the retina and serum

Retinal isolation, processing for sterol quantifications, and sterol quantifications were carried out as described [66, 70]. Unesterified cholesterol, lathosterol and desmosterol along with total cholesterol (a sum of esterified and unesterified cholesterol) were measured in individual retinas by isotope dilution gas chromatography–mass spectroscopy (GC–MS) using deuterated sterol analogs as internal standards [66, 70]. Cholesterol in the serum was measured as total and free sterol after animals were fasted overnight and their blood was withdrawn via cardiac puncture followed by serum isolation as described [71].

Quantitative RT-PCR (qRT-PCR)

Retinas from 5 to 7 mice per genotype were combined, and total RNA was isolated by the TRIzol Reagent (Life Technologies) according to the manufacturer's instructions. This RNA (1 µg) was then converted to cDNA by SuperScript III reverse transcriptase (Invitrogen) according to manufactures instructions. qRT-PCR was performed as described [66, 69] in triplicate on an LightCycler 480 instrument (Roche Life Science) using cDNA, a pair of gene-specific primers (Suppl. Table S1), and a FastStart Universal SYBR Green Master (Rox) (Roche Diagnostics, #04913850001); Gapdh served as a reference gene. Changes in the relative mRNA levels were calculated by the $2^{-\Delta\Delta C_t}$ method [72].

Glucose tolerance test

Mice were fasted overnight after their beddings were removed and injected with a solution of 25% D-glucose (2 g/kg body weight, Sigma-Aldrich, G7528) into the peritoneum. The blood was withdrawn from the tail vein and assayed for glucose by an Elite XL Glucometer (Bayer Contour) before and after the injection (30, 60, 120, and 150 min) at least in triplicate for each time point.

Retinal proteomics

The label-free approach was used as described [6]. Briefly, four biological replicates per genotype, each representing three 6–8-month-old male mice, one retina from a mouse, were frozen, cryo-pulverized, and lysed with 3% SDS. Samples were then cleaned of detergent and alkylated with iodoacetamide. Proteins were sequentially digested with lysyl endopeptidase and trypsin (Wako Chemicals, #125-05061 and 9002-07-7, respectively), and an equal amount of internal standard (Pierce Retention Time Calibration Mixture 88321, Thermo Fisher Scientific) was added to each sample. Digested proteins were analyzed by LC/MS/MS carried out on a LTQ-Orbitrap Velos mass spectrometer (Thermo Fisher Scientific) equipped with a nanoAcquity™ ultra-high-pressure liquid chromatography system (Waters). Blank injections were run after each sample to minimize carryover between samples. Full-scan MS spectra (m/z 380–1800) were acquired at a resolution of 60,000 at m/z 400 followed by 20 data-dependent MS/MS scans generated in the ion-trap detector by collision-induced dissociation of the peptide ions. The data obtained were searched against the mouse Uniprot database (538,585 sequences). Differences in relative protein abundance were calculated by the PEAKS software (Bioinformatics Solutions Inc) based on unique peptides [73]. Proteins with non-significant changes ($P \geq 0.05$) in abundance between the genotypes were excluded from the subsequent proteomics analysis as are the proteins with less than 2 unique peptides/protein and a 1.5-fold change in the relative abundance, even if this change was significant. Protein grouping was based on protein function described in literature (Suppl. T1).

Transmission electron microscopy (TEM)

The retina was fixed in a quarter strength of the Karnovsky's fixative (4% paraformaldehyde and 5% glutaraldehyde in 0.1 M Na cacodylate, pH 7.4 [74] and then sequentially post-fixed in 3% glutaraldehyde in 0.1 M Na cacodylate buffer, pH 7.4; 1% OsO_4 in 0.1 M Na cacodylate buffer, pH 7.4; 1% tannic acid in 0.05 M Na cacodylate, pH 7.4; and 1% paraphenylenediamine in 70% ethanol. Images were examined by a 1200EX transmission electron microscope (JEOL Ltd.).

Metabolic fluxes of retinal glucose in vivo

Mice were fasted overnight in clean cages without the bedding material. The next morning mice were injected intraperitoneally with 0.2 ml of 200 mg/ml solution of D-[U-^{13}C]glucose (Cambridge Isotope Laboratories Inc., CLM-1396-PK) in saline, i.e., 40 mg of [U-^{13}C]glucose/mouse. Animals were sacrificed 30 min post-injection and their serum and retinas were collected. Glucose isotopic enrichment in the serum was determined as described [75] with modifications. Briefly, glucose was extracted from 50 µl of serum collected from individual animals by addition of 500 µl of ice-cold ethanol containing the internal standard (D-[6,6-$^2H_2$]-glucose, Cambridge Isotope Laboratories Inc., DLM-349-PK). Samples were mixed and incubated on ice for 30 min followed by centrifugation at 4 °C for 10 min at 14,000g. The supernatants obtained were transferred to the GC–MS vials and evaporated to dryness. Acetic anhydride (150 µl) in pyridine (2:1, vol/vol) was added to the vials to convert glucose to pentaacetate derivative by reacting at 60 °C for 30 min. Solutions were evaporated to dryness and reconstituted in 80 µl of ethyl acetate. Samples were transferred to the GC–MS inserts and crimped. Sample volume of 1 µl was injected into GC–MS, and sample analyses were performed in duplicate. The m/z values of 331(M0) and 337 (M6) were monitored, and glucose enrichment was calculated as a ratio of (M6)/(ΣM0 + M6). The glucose concentration was calculated based on a calibration curve ($y = 5.242 + 0.6733$, $R^2 = 0.9937$) and a ratio of (ΣM0–M6) to M2, the D-[$^2H_2$]-glucose internal standard. In the retina, the glucose concentrations and isotopic enrichment were measured using pooled samples of two retinas from one mouse. Retinas were homogenized in 4 ml of chloroform–methanol mixture (2:1, vol/vol) followed by centrifugation at 4 °C for 10 min at 14,000g. The supernatants were mixed with 1 ml of water and homogenized again. The second centrifugation (4 °C, 10 min, 14,000g) was carried out, and the upper layers were taken and evaporated to dryness. Extracts were reconstituted in 1 ml of 80% ethanol, and 200 µl of these extracts were processed to determine glucose enrichment and concentration as described for the serum. The rest of the extracts was used to determine glucose metabolites. Solutions were transferred to GC–MS vials and evaporated to dryness under a gentle stream of nitrogen. Keto- and aldehyde groups were reduced by addition of 10 µl of 1 N NaOH and 15 µl NaB_2H_4 (prepared as 10 mg/ml in 50 mM NaOH stock). Samples were mixed and incubated at room temperature for 1 h followed by acidification with 55 µl of 1 N HCl by dropping the acid slowly to avoid deuterium loss. Samples were then evaporated to dryness, and 50 µl of methanol was added to precipitate boric acid. The internal standard (10 µl of 0.1 mg/ml heptadecanoic acid (MilliporeSigma, #H3500) in methanol was added, and samples were evaporated to dryness. Dried extracts were derivatized in 40 µl of pyridine and 60 µl of *tert*-butylbis(dimethylsilyl) trifluoroacetamide with 10% trimethylchlorosilane (Regisil, Regis Technologies, #1-270111-200) at 60 °C for 1 h. The resulting derivatives were injected into an Agilent 5973 mass spectrometer equipped with an Agilent 6890 Gas Chromatograph. A HP-5MS capillary column (60 m × 0.25 mm × 0.25 µm, Agilent Technologies, Santa Clara, CA) was used for all runs with a helium flow of 1.5 ml/min. Samples were analyzed in

selected ion monitoring mode using electron impact ionization; the ion dwell time was set to 10 ms. Fractional glucose metabolic flux was calculated as a ratio of a molar percent enrichment of the product to a molar percent enrichment of the precursor. Relative metabolite concentrations were determined as a ratio of metabolite abundance to standard abundance. Absolute metabolic rate was determined as a product of fractional metabolic flux and pool size, i.e., relative concentration of metabolite of interest.

Statistical analyses

All images are representative of studies in three to five animals per genotype unless otherwise indicated. All quantitative data represent the mean ± SD or the mean ± SEM; the sample size is indicated in each figure or figure legend. Data were analyzed either by a two-tailed, unpaired Student's *t* test, two-way repeated measures ANOVA or two-way ANOVA with Bonferroni correction. The GraphPad Prism software (GraphPad) was used. Statistical significance was defined as $*P \leq 0.05$; $**P \leq 0.01$; $***P \leq 0.001$; $****P \leq 0.0001$.

Results

Retinal APOD immunolocalization

The retina of *ApoD*$^{-/-}$ mice was used as a major negative control (Fig. 1). In wild-type (C57BL/6J) mice, the immunoreactivity for APOD was mainly detected in the photoreceptor inner segments (IS), and in addition, in some cells of the ganglion cell layer and inner nuclear layer. Such a confined pattern of the APOD immunolocalization suggested a particular apolipoprotein importance for the IS.

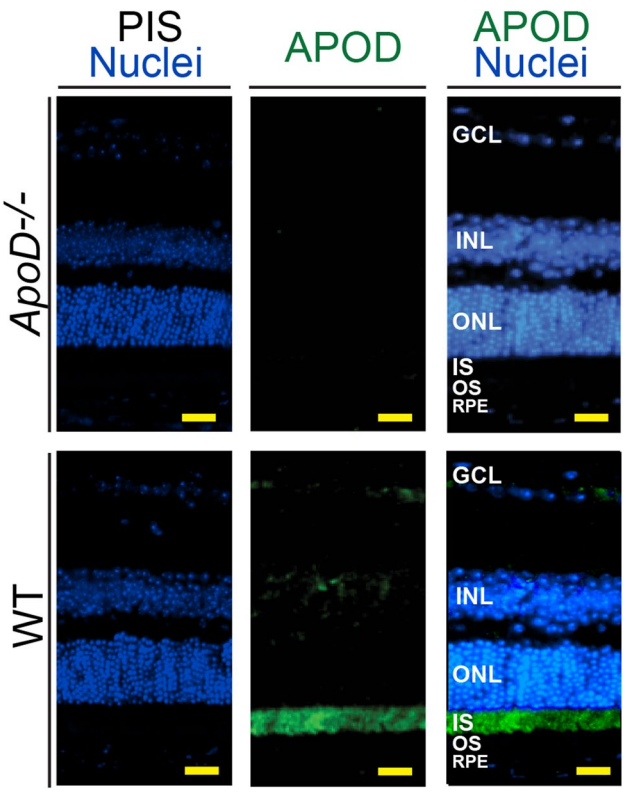

Fig. 1 Immunolocalization of APOD in mouse retina. Nuclei are in blue (stained with DAPI), and immunoreactivity for APOD is in green. *PIS* preimmune serum, used as control stains. *GCL* ganglion cell layer, *INL* inner nuclear layer, *ONL* outer nuclear layer, *IS* photoreceptor inner segments, *OS* photoreceptor outer segments, *RPE* retinal pigment epithelium, *WT* wild type (C57BL/6J). All images are representative: $n = 3$ mice (6–8 months old) per genotype. *Scale bars* 50 µm

Serum and retinal sterol quantifications

Both sexes of four genotypes were characterized (Fig. 2a–d), and sex differences were found only in *ApoE*$^{-/-}$ mice in the levels of serum sterols. In *ApoD*$^{-/-}$ mice of both sexes, the levels of total serum and retinal cholesterol were unchanged as compared to wild-type animals. In *ApoD*$^{-/-}$*ApoE*$^{-/-}$ mice of both sexes, the levels of total serum cholesterol were increased and were higher than those in the individual knockouts. Nevertheless the retinal cholesterol content was normal in *ApoD*$^{-/-}$*ApoE*$^{-/-}$ mice despite the increased content in *ApoE*$^{-/-}$ mice. Retinal lathosterol and desmosterol provide insight in the rate of cholesterol biosynthesis in neurons and astrocytes, respectively [76, 77]. The levels of both sterols were unchanged in the *ApoD*$^{-/-}$ retina and increased in the *ApoD*$^{-/-}$*ApoE*$^{-/-}$ retina, probably a contribution of the *ApoE*$^{-/-}$ genotype, in which both retinal lathosterol and desmosterol were increased. Thus, in wild-type mice, APOD does not appear to be a major contributor to retinal cholesterol maintenance. Conversely, in *ApoE*$^{-/-}$ mice, APOD is a negative contributor to retinal cholesterol homeostasis as *ApoD* ablation had a normalizing effect on retinal sterols as compared to *ApoE*$^{-/-}$ mice.

Retinal distribution of cholesterol

Only unesterified (free) cholesterol was studied, because the levels of esterified cholesterol were very low in the *ApoD*$^{-/-}$ and *ApoD*$^{-/-}$*ApoE*$^{-/-}$ retinas (Fig. 2b). Incubations with filipin, a fluorescent antibiotic and validated stain for retinal cholesterol [67, 78], revealed that overall, the *ApoD*$^{-/-}$ retina had very similar filipin fluorescence as compared to the wild-type retina (Fig. 2e, f). The only exception was a region of the photoreceptor outer segments adjacent to the retinal pigment epithelium (RPE) and the basal membrane of the RPE, which appeared to have a more intense fluorescent signal. Yet, the *ApoD*$^{-/-}$*ApoE*$^{-/-}$ retina

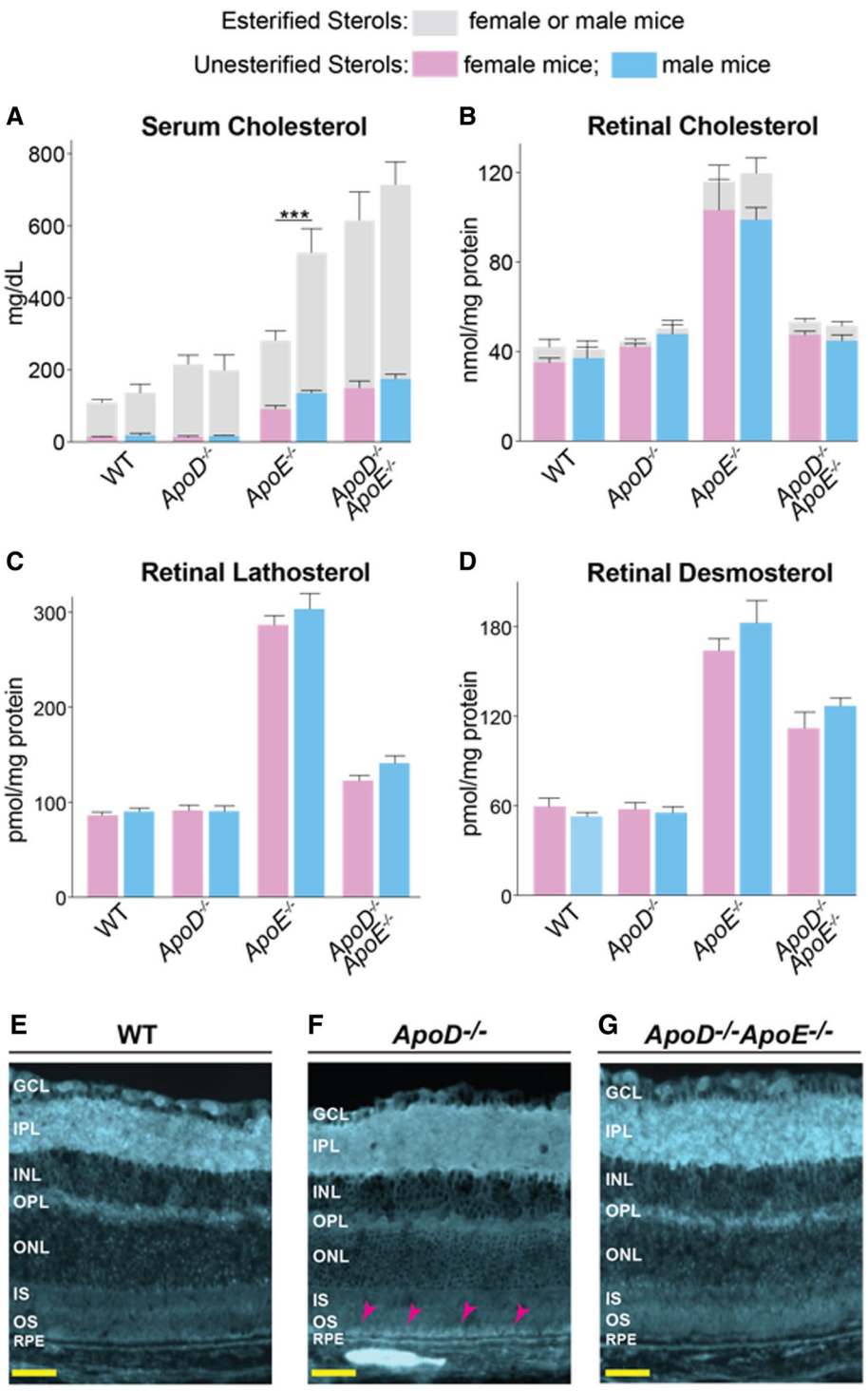

Fig. 2 Serum and retinal sterols. **a–d**, Sterol quantifications. Results are mean ± SD of the measurements in individual mice (3–6 animals/genotype/sex; number of mice equals the number of retinas); animals were 6-months old. Statistical significance was assessed by two-way ANOVA with Bonferroni correction. Black line and asterisk indicate statistically significant differences between sexes of the same genotype; the results of all other comparisons are summarized in Supplemental Tables S2–S5. ***$P \leq 0.001$. **e–g** Retinal distribution of unesterified cholesterol as assessed by filipin (cyan) staining. All images are representative: $n = 3$ mice per genotype. *Scale bars* 50 µm. *GCL* ganglion cell layer, *IPL* inner plexiform layer, *INL* inner nuclear layer, *OPL* outer plexiform layer, *ONL* outer nuclear layer, *IS* photoreceptor inner segments, *OS* photoreceptor outer segments, *RPE* retinal pigment epithelium, *WT* wild type

did not seem to have these changes (Fig. 2g), and its pattern of filipin staining was similar to that of wild type mice.

Retinal in vivo characterizations

Mice were first evaluated by SD-OCT and doppler flow SD-OCT (Fig. 3). Examination in cross-section showed that some of the 6 month old $ApoD^{-/-}$ but not $ApoD^{-/-}ApoE^{-/-}$ mice had small elevations of the RPE and the blood flow in the outer retina in the area of these elevations—changes suggestive of pathologic choroidal neovascularization [79]. Hence, FI and FA were carried out so that in the latter, the laser beam was focused either on the inner or outer retina, and images were captured at the

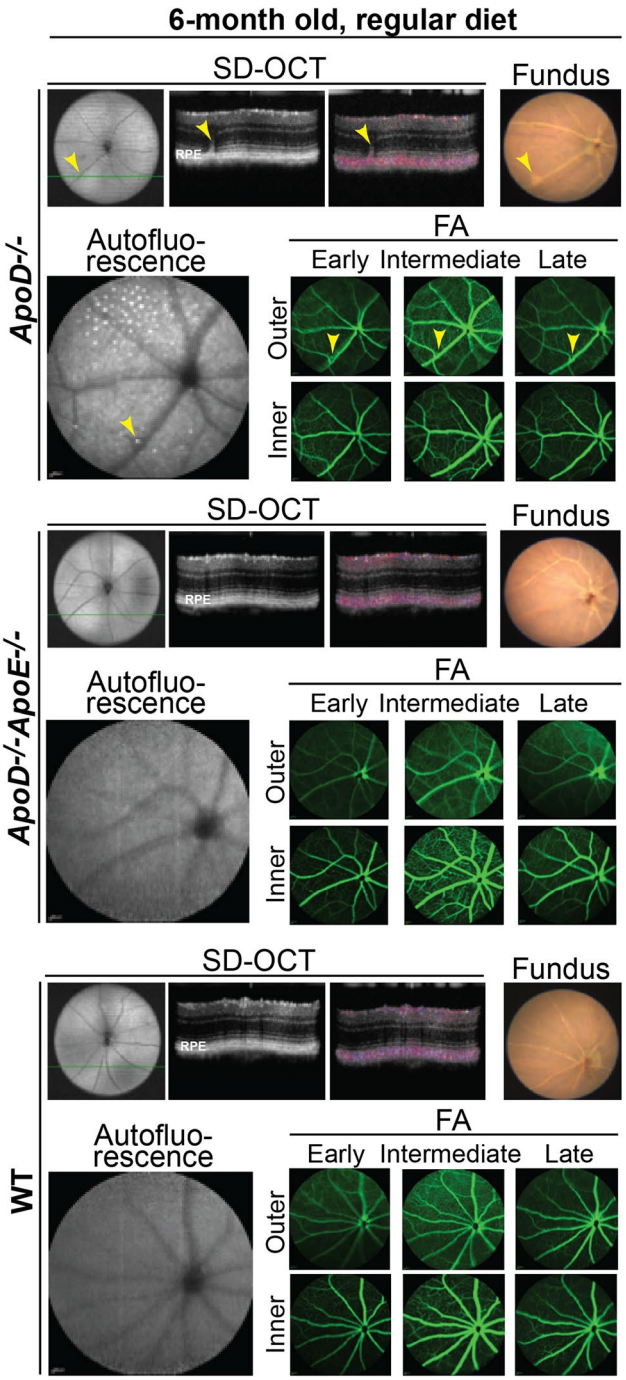

Fig. 3 Retinal in vivo imaging of mice on regular diet. Representative ($n = 5$/genotype) assessments by spectral domain-optical coherence tomography (SD-OCT), fundus color imaging (Fundus), fundus autofluorescence (Autofluorescence), and fundus fluorescein angiography (FA) after an injection with sodium fluorescein. The SD-OCT panels show a fundus image and two retinal cross-sections (from left to right), the latter is a Doppler flow, which reflects the direction of the blood flow. The FA panels show an early, intermediate and late stage fundus fluorescence (from left to right) with the laser beam being focused either on the outer (Outer) or inner (Inner) retina. Yellow arrowheads point to retinal abnormalities. No sex-based differences were detected, hence only images of male mice are shown

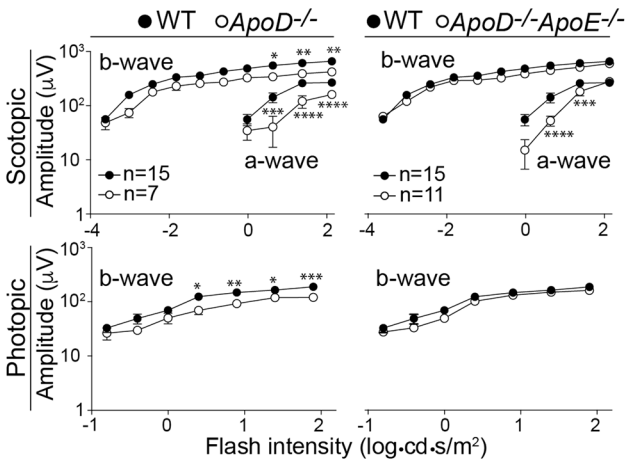

Fig. 4 Electroretinography responses in 6-month-old male mice. Results are mean ± SEM of the measurements in 7–15 animals; the number of animals (n) is indicated in each upper panel. Statistical significance was assessed at various light intensities for two mouse genotypes by repeated measures two-way ANOVA with Bonferroni's correction for multiple comparisons. $^{*}P \le 0.05$; $^{**}P \le 0.01$; $^{***}P \le 0.001$; $^{****}P \le 0.0001$

early, intermediate and late FA stages. The lesion area in *ApoD*$^{-/-}$ mice was presented as a large yellow spot on FI and a hyperfluorescent spot on FA. This hyperfluorescent spot was observed in the outer retina with the brightest hyperfluorescence being at the intermediate FA stage. Such a hyperfluorescence pattern supports choroidal neovascularization and is consistent with increased permeability of the newly grown pathologic blood vessels. Also, *ApoD*$^{-/-}$ mice had multiple autofluorescent spots, one in the area of neovascularization and others outside of this area. Retinal assessment by ERGs showed that the amplitudes of both scotopic and photopic ERGs were decreased in *ApoD*$^{-/-}$ mice indicating impaired retinal function (Fig. 4). Yet, in the *ApoD*$^{-/-}$*ApoE*$^{-/-}$ retina, only one amplitude, namely that of the scotopic a-wave, was reduced and could be an indicator of a disturbance in the rod photoreceptor function [80]. Thus, *ApoD*$^{-/-}$ mice had a more prominent retinal phenotype than *ApoD*$^{-/-}$*ApoE*$^{-/-}$ mice.

Retinal proteomics

This was conducted to gain insights into the mechanisms that might contribute to retinal vascular abnormalities and impaired retinal function in *ApoD*$^{-/-}$ mice as well as the normalization of retinal cholesterol and function in *ApoD*$^{-/-}$*ApoE*$^{-/-}$ mice. The label-free analysis was used, and each knockout genotype was compared to wild type mice. A total of 54 and 36 proteins with differential abundance were identified in the *ApoD*$^{-/-}$ and *ApoD*$^{-/-}$*ApoE*$^{-/-}$ retinas, respectively (Tables 1, 2). In the former, 28 and 26 proteins were upregulated and downregulated, respectively; in the latter, 16 and 20 proteins were upregulated and downregulated,

Table 1 Differentially abundant proteins (more than a 1.5-fold change) in the *ApoD*$^{-/-}$ (KO) vs C57BL/6J (WT) retina

Protein	No. of peptides with significant changes in abundance	No. of unique peptides	Sequence coverage (%)	Peptide intensity (a.u.) × 10^6		KO/WT, protein ratio
				KO	WT	
Genetic information transfer						
FBLL1	3	2	17	0.57 ± 0.09	0.30 ± 0.20	1.9
GPTC8	**2**	**2**	**2**	**0.04 ± 0.02**	**0.09 ± 0.03**	**0.4**
NIPBL	2	2	1	0.42 ± 0.11	0.13 ± 0.15	3.2
NR2E3	6	6	26	1.83 ± 0.31	0.93 ± 0.31	2.0
PDS5A	3	3	5	0.36 ± 0.06	1.73 ± 0.32	2.1
PPIL1	4	4	45	1.98 ± 0.31	1.14 ± 0.62	1.7
PRPF3	**4**	**4**	**7**	**0.64 ± 0.42**	**1.69 ± 0.47**	**0.4**
RBM26	**7**	**6**	**10**	**1.04 ± 0.55**	**1.87 ± 0.40**	**0.6**
RBM3	7	7	63	12.73 ± 2.67	8.18 ± 0.56	1.6
RL34	**4**	**4**	**21**	**3.39 ± 0.50**	**5.10 ± 0.36**	**0.7**
RS9	**8**	**8**	**34**	**7.94 ± 2.20**	**13.17 ± 2.50**	**0.6**
TCP4	**3**	**3**	**26**	**42.03 ± 12.21**	**69.63 ± 2.80**	**0.6**
VIGLN	**21**	**21**	**22**	**3.76 ± 1.34**	**10.91 ± 5.11**	**0.3**
Vesicular traffic						
ARFG1	**7**	**7**	**36**	**1.25 ± 0.30**	**2.33 ± 0.80**	**0.5**
COPA	**28**	**28**	**29**	**3.21 ± 0.72**	**5.03 ± 0.18**	**0.6**
EXOC4	**2**	**2**	**3**	**0.57 ± 0.19**	**0.97 ± 0.20**	**0.6**
FLOT1	2	2	7	0.68 ± 0.17	0.38 ± 0.10	1.8
LCAP	**2**	**2**	**3**	**0.1 ± 0.02**	**0.32 ± 0.05**	**0.3**
LTOR3	2	2	31	0.99 ± 0.39	0.39 ± 0.06	2.6
MAP1S	6	6	11	1.0 ± 0.15	0.64 ± 0.12	1.6
NCLN	7	7	17	1.48 ± 0.40	0.96 ± 0.17	1.6
PA1B2	5	5	42	12.80 ± 2.01	8.81 ± 1.23	1.5
RAB4B	**4**	**2**	**25**	**0.66 ± 0.47**	**1.37 ± 0.29**	**0.5**
VALT	2	2	32	16.30 ± 5.89	7.16 ± 4.75	2.3
WIPI1	2	2	9	0.55 ± 0.10	0.29 ± 0.15	1.9
Inflammation						
SERPINA1E	**10**	**4**	**35**	**1.35 ± 0.89**	**3.61 ± 1.44**	**0.4**
ANM5	6	6	19	1.87 ± 0.33	1.22 ± 0.21	1.5
AQP4	3	3	14	6.11 ± 0.73	3.48 ± 1.5	1.8
CLIC6	**10**	**10**	**30**	**0.96 ± 0.27**	**2.16 ± 0.32**	**0.4**
DDRGK	2	2	10	0.36 ± 0.03	0.21 ± 0.09	1.7
HPT	**4**	**4**	**14**	**0.15 ± 0.13**	**1.12 ± 0.41**	**0.1**
IFIT3	**2**	**2**	**4**	**0.09 ± 0.02**	**0.93 ± 0.38**	**0.1**
TRAFD1	3	3	8	1.34 ± 0.24	0.85 ± 0.18	1.6
VMA5A	5	5	9	1.45 ± 0.08	0.89 ± 0.25	1.6
WDFY1	4	4	12	1.25 ± 0.68	0.40 ± 0.09	3.1
Metabolism						
ALDR	14	14	51	9.92 ± 1.90	5.66 ± 1.28	1.8
GALE	3	3	15	1.00 ± 0.19	0.58 ± 0.11	1.7
INO1	7	7	18	2.48 ± 0.37	1.49 ± 0.59	1.7
PUR2	8	8	14	2.52 ± 0.72	1.64 ± 0.18	1.5
RET1	**10**	**10**	**75**	**5.93 ± 1.14**	**10.17 ± 1.67**	**0.6**
Cellular adhesion						
E41L5	4	4	10	1.43 ± 0.22	0.62 ± 0.16	2.3
PDLI3	**2**	**2**	**16**	**0.05 ± 0.09**	**0.53 ± 0.25**	**0.1**
TINAL	3	3	12	0.59 ± 0.18	0.32 ± 0.09	1.8

Table 1 (continued)

Protein	No. of peptides with significant changes in abundance	No. of unique peptides	Sequence coverage (%)	Peptide intensity (a.u.) × 10^6		KO/WT, protein ratio
				KO	WT	
TLN2	**35**	**32**	**24**	**4.50 ± 0.99**	**8.94 ± 3.24**	**0.5**
Mitochondrial function						
CLPP	**2**	**2**	**10**	**0.40 ± 0.05**	**0.71 ± 0.06**	**0.6**
NUDT9	**2**	**2**	**6**	**0.14 ± 0.12**	**0.65 ± 0.23**	**0.2**
PPIF	2	2	17	0.87 ± 0.19	0.51 ± 0.14	1.7
SAHH2	**14**	**8**	**35**	**12.77 ± 6.79**	**24.80 ± 5.20**	**0.5**
Ciliogenesis						
C2D2A	**2**	**2**	**1**	**0.01 ± 0.004**	**0.04 ± 0.01**	**0.3**
DC1I1	2	2	6	0.78 ± 0.11	0.49 ± 0.17	1.6
SYNE2	**3**	**2**	**<1**	**0.57 ± 0.19**	**0.97 ± 0.20**	**0.6**
Synaptic function						
CAC1A	**2**	**2**	**1**	**0.26 ± 0.06**	**0.44 ± 0.03**	**0.6**
RIMS2	**2**	**2**	**1**	**0.02 ± 0.01**	**0.05 ± 0.02**	**0.4**
PLST	8	6	22	1.66 ± 0.18	1.12 ± 0.27	1.5

Protein grouping is by process and shows each protein only in one group despite the involvement in multiple processes. Proteins with a decreased expression are in bold

respectively. When these proteins were grouped by function (Suppl. T1), at least eight biological processes were identified as potentially affected in each of the knockout genotypes. Seven of these processes were the same in the *ApoD*$^{-/-}$ and *ApoD*$^{-/-}$*ApoE*$^{-/-}$ retinas, although the affected proteins and their number were different in the two knockouts. The commonly affected processes included: genetic information transfer (Suppl. Figs. S1, S2), vesicular traffic (Suppl. Figs. S3, S4), metabolism (Suppl. Figs. S5, S6), cellular adhesion (Suppl. Figs. S1, S2), mitochondrial function (Suppl. Figs. S5, S6), ciliogenesis (Suppl. Figs. S1, S2), and synaptic function (Suppl. Figs. S1, S2). One of the affected processes was specific to each genotype, namely inflammation in the *ApoD*$^{-/-}$ retina (Supl. Fig. S1) and protein folding in the *ApoD*$^{-/-}$*ApoE*$^{-/-}$ retina (Suppl. Fig. S2). Of the proteins with unaltered expression, 13 (APOAs 1, 2, 4, E and J, DHCR7, LRP1, LRPAP1, MESD, MSMO1, NCEH1, OSBL1, and OSBP1) in the *ApoD*$^{-/-}$ retina and 9 (APOAs 2 and J, EBP, LRP1, LRPAP1, MESD, NCEH1, OSBL1, and SCAP) in the *ApoD*$^{-/-}$*ApoE*$^{-/-}$ retina were of importance for cholesterol homeostasis (Supl. Text T1; Suppl. Tables S6, S7). Unaltered expression of these proteins was consistent with unaltered retinal sterol profile in *ApoD*$^{-/-}$ mice (Fig. 2) and pointed to the non-conventional mechanism(s) of cholesterol removal in *ApoD*$^{-/-}$*ApoE*$^{-/-}$ mice. Therefore, next, we used TEM to examine retinal ultrastructure for the presence of vesicles as vesicular formation was previously identified to serve a reserve mechanism for retinal cholesterol removal [81]. In addition, vesicular formation was suggested as potentially affected in the *ApoD*$^{-/-}$ retina by retinal proteomics (Suppl. Figs. S3, S4). We also used TEM to assess mitochondrial morphology as retinal proteomics pointed to changes in the metabolism and mitochondrial function (Suppl. Figs. S5, S6).

TEM

The main focus was on the photoreceptors as their inner segments are highly abundant in mitochondria and were also found to be the major site of APOD immunolocalizations (Fig. 1). Intracellular vesicles, individual or in multivesicular bodies, were indeed found in the wild type and knockout genotypes and appeared to be more abundant in the *ApoD*$^{-/-}$*ApoE*$^{-/-}$ than the *ApoD*$^{-/-}$ and wild-type retinas (Fig. 5). In addition, authophagosomes were readily detectable in the retina of *ApoD*$^{-/-}$*ApoE*$^{-/-}$ mice and could reflect enhanced autophagosome formation suggested by the retinal proteomics (Suppl. Fig. S4). As for the mitochondria, all the genotypes (wild type, *ApoD*$^{-/-}$, and *ApoD*$^{-/-}$*ApoE*$^{-/-}$ mice) appeared to have mitochondrial pinching (Fig. 5) which usually occurs during mitochondrial fission or fusion, the processes in the maintenance of healthy mitochondria [82]. Pinching seemed to be more frequent in the *ApoD*$^{-/-}$ than the wild type and *ApoD*$^{-/-}$*ApoE*$^{-/-}$ retinas and could represent the mitochondrial response to increased metabolic or environmental stress [82]. Some of the mitochondria in the *ApoD*$^{-/-}$ retina appeared to be ruptured, an insult that was not observed in either the wild type or *ApoD*$^{-/-}$*ApoE*$^{-/-}$ retinas. Also, wavy plasma membranes were observed in the *ApoD*$^{-/-}$ genotype in the regions of mitochondrial alignment, the change that was not present in wild type mice and was minimal in *ApoD*$^{-/-}$*ApoE*$^{-/-}$ mice. Such a cellular

Table 2 Differentially abundant proteins (more than a 1.5-fold change) in the *ApoD*$^{-/-}$*ApoE*$^{-/-}$ (DKO) vs C57BL/6J (WT) retina

Protein	No. of peptides with significant changes in abundance	No. of unique peptides	Sequence coverage (%)	Peptide intensity (a.u.)×10^6		DKO/WT, protein ratio
				DKO	WT	
Protein folding						
CALU	8	8	45	11.33 ± 0.91	7.56 ± 1.82	1.5
CRBA2	**7**	**7**	**43**	**13.44 ± 14.31**	**75.30 ± 32.74**	**0.2**
CRBA4	**6**	**6**	**49**	**12.80 ± 12.65**	**75.25 ± 39.22**	**0.2**
CRBB1	**6**	**6**	**37**	**17.72 ± 17.07**	**88.00 ± 43.01**	**0.2**
CRBB2	**11**	**11**	**53**	**145 ± 150**	**760 ± 289**	**0.2**
CRBB3	**11**	**11**	**61**	**13.43 ± 10.96**	**64.53 ± 30.48**	**0.2**
CRYAA	**8**	**8**	**54**	**266 ± 211**	**1,600 ± 462**	**0.2**
CRYAB	**8**	**8**	**63**	**100 ± 108**	**456 ± 120**	**0.2**
Mitochondrial function						
HBA	**6**	**6**	**43**	**568 ± 110**	**882 ± 178**	**0.6**
HBB1	**8**	**8**	**61**	**686 ± 112**	**1,086 ± 135**	**0.6**
NU5M	4	4	9	12.00 ± 1.57	7.57 ± 2.86	1.6
PHB	**10**	**10**	**47**	**16.35 ± 5.72**	**41.90 ± 16.48**	**0.4**
WFS1	3	3	4	1.15 ± 0.06	0.42 ± 0.27	2.8
Synaptic function						
CA2D1	4	4	6	2.03 ± 0.13	0.80 ± 0.58	2.5
DAG1	2	2	5	1.48 ± 0.31	0.73 ± 0.39	2.0
DLG1	**9**	**7**	**17**	**2.57 ± 0.29**	**4.10 ± 0.89**	**0.6**
RING2	2	2	9	1.26 ± 0.13	0.86 ± 0.23	1.5
VAMP2	4	2	35	33.18 ± 0.25	22.95 ± 1.03	1.5
Vesicular traffic						
CAV1	2	2	20	4.69 ± 0.12	3.22 ± 0.83	1.5
EPS15L1	6	6	11	3.16 ± 0.13	2.18 ± 0.13	1.5
TPP1	3	3	7	5.69 ± 0.83	2.80 ± 1.85	2.0
TWF1	5	5	23	3.79 ± 0.42	2.26 ± 0.32	1.7
YKT6	2	2	20	2.48 ± 0.38	1.69 ± 0.21	1.5
Ciliogenesis						
BBS7	5	5	10	3.50 ± 0.32	2.24 ± 0.33	1.6
CENT2	2	2	27	2.40 ± 0.51	1.44 ± 0.59	1.7
GELS	**2**	**2**	**6**	**2.26 ± 0.49**	**4.11 ± 0.99**	**0.5**
PDE6D	4	4	33	13.90 ± 4.45	7.22 ± 2.12	1.9
Genetic information transfer						
CAPR1	**7**	**7**	**23**	**24.91 ± 18.77**	**107.45 ± 47.76**	**0.2**
IF4A2	**13**	**8**	**47**	**18.30 ± 5.81**	**42.15 ± 15.29**	**0.4**
PPM1G	2	2	8	1.98 ± 0.31	1.27 ± 0.25	1.6
RUVB2	**11**	**11**	**27**	**9.17 ± 3.21**	**19.2 ± 6.68**	**0.5**
Metabolism						
ALBU	**10**	**10**	**20**	**102 ± 13**	**189 ± 26**	**0.6**
APOA1	**3**	**3**	**12**	**3.04 ± 0.89**	**7.61 ± 0.78**	**0.4**
FABP5	**2**	**2**	**16**	**4.92 ± 3.74**	**18.95 ± 7.81**	**0.3**
KT3K	**5**	**5**	**17**	**3.12 ± 0.62**	**5.17 ± 0.51**	**0.6**
Cellular adhesion						
VINC	**9**	**9**	**14**	**18.00 ± 22.99**	**87.65 ± 32.03**	**0.2**

Protein grouping is by process and shows each protein only in one group despite the involvement in multiple processes. Proteins with a decreased expression are in bold

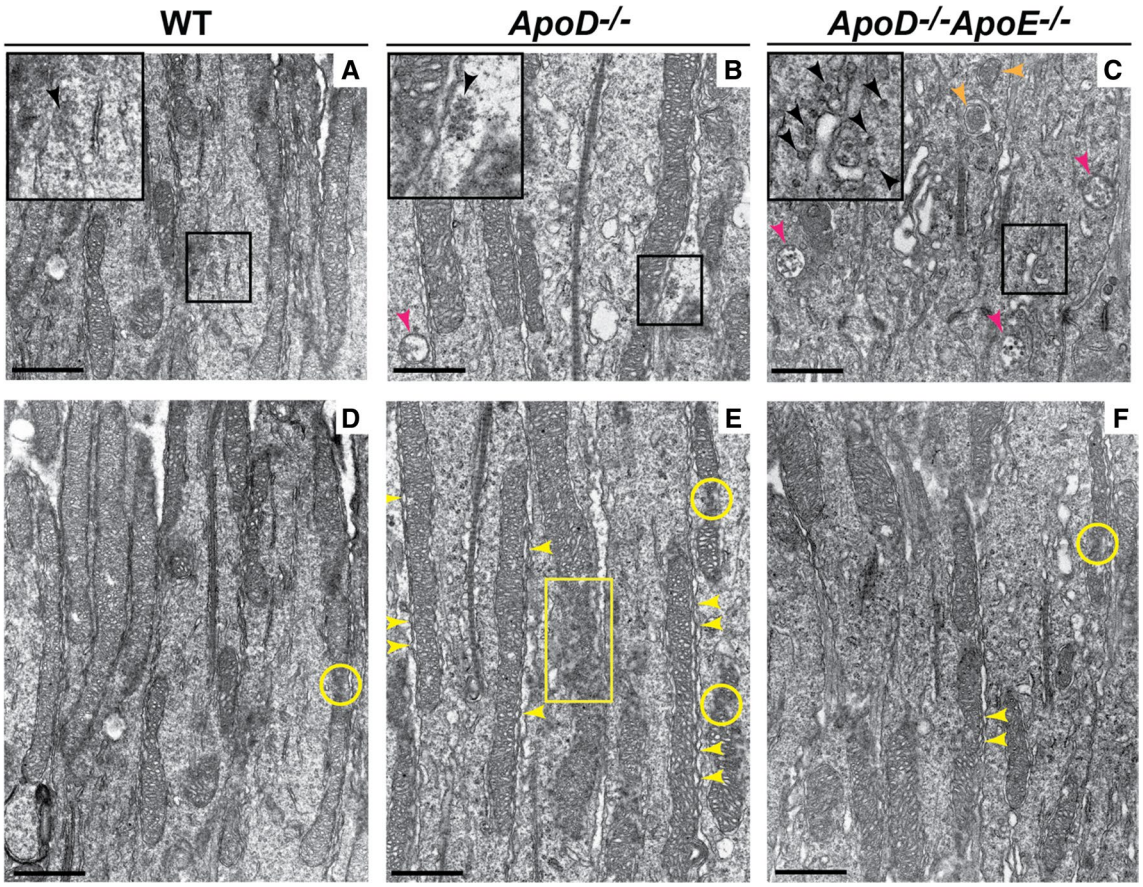

Fig. 5 Retinal ultrastructure as assessed by transmission electron microscopy. Longitudinal cross-sections through the photoreceptor inner segments are shown. **a**–**c** Black rectangles indicate regions that are shown at a higher magnification in the upper left corner. Black and magenta arrowheads point to individual intracellular vesicles or multivesicular bodies, respectively. Orange arrowheads point to autophagosomes. **d**–**f**, Yellow circles indicate mitochondrial pinching, yellow rectangle indicates mitochondrial rupture, yellow arrowheads indicate wavy plasma membranes. Images are representative of two male mice per genotype; all mice were 7-months old. *Scale bars* 1 µm

membrane deformation is consistent with changes in the endocytosis suggested by the retinal proteomics (Suppl. Figs. S3, S4) and is typically associated with the redistribution of membrane-bound proteins [83]. Thus, studies by TEM provided evidence for increased mitochondrial stress in the *ApoD*$^{-/-}$ retinas and increased autophagosome as well as vesicular formation in the *ApoD*$^{-/-}$*ApoE*$^{-/-}$ retinas, consistent with the implications by retinal proteomics.

Retinal gene expression and immunohistochemistry

We hypothesized that the APOD effects on the retina are realized, at least in part, via the receptors for APOD and subsequent intracellular signaling (Fig. 6a, d). Hence, we quantified retinal expression of the four genes for the APOD receptors: *Bsg1* and *Bsg2* encoding the two isoforms of BASI, *Lepr* encoding OB-Rb, and *Scarb1* encoding SR-B1 [27–29]. We also measured mRNA of RdCVF, rod-derived cone viability factor, that acts through binding to BASI [84]. Of these five genes, the major changes in the expression were found only for *Lepr*, 11.7- and 5.9-fold increases in the *ApoD*$^{-/-}$ and *ApoD*$^{-/-}$*ApoE*$^{-/-}$ retina, respectively (Fig. 6a). Hence, a confirmatory retinal OB-Rb immunolocalization was carried out and documented the predominant OB-Rb expression in the IS in wild type mice (Fig. 6b). In the *ApoD*$^{-/-}$ and *ApoD*$^{-/-}$*ApoE*$^{-/-}$ retina, the immunoreactivity for OB-Rb was present in the IS as well and seemed to be more intense than that in the wild-type retina, consistent with the mRNA measurements. In addition, the anti-OB-Rb signal was present in the ganglion cell layer, inner nuclear layer, and outer plexiform layer in the knockout genotypes. OB-Rb is a regulator of fatty acid and glucose metabolism in the brain, muscle, and adipose tissue [31], and glucose metabolism was suggested to be affected in the *ApoD*$^{-/-}$ retina by the proteomics approach (Table 1, Suppl. Figs. S3, S5). Therefore, we measured retinal mRNA expression of *Glut1*, *Glut2*, *Glut 3*, and *Glut4*, the four glucose transporters.

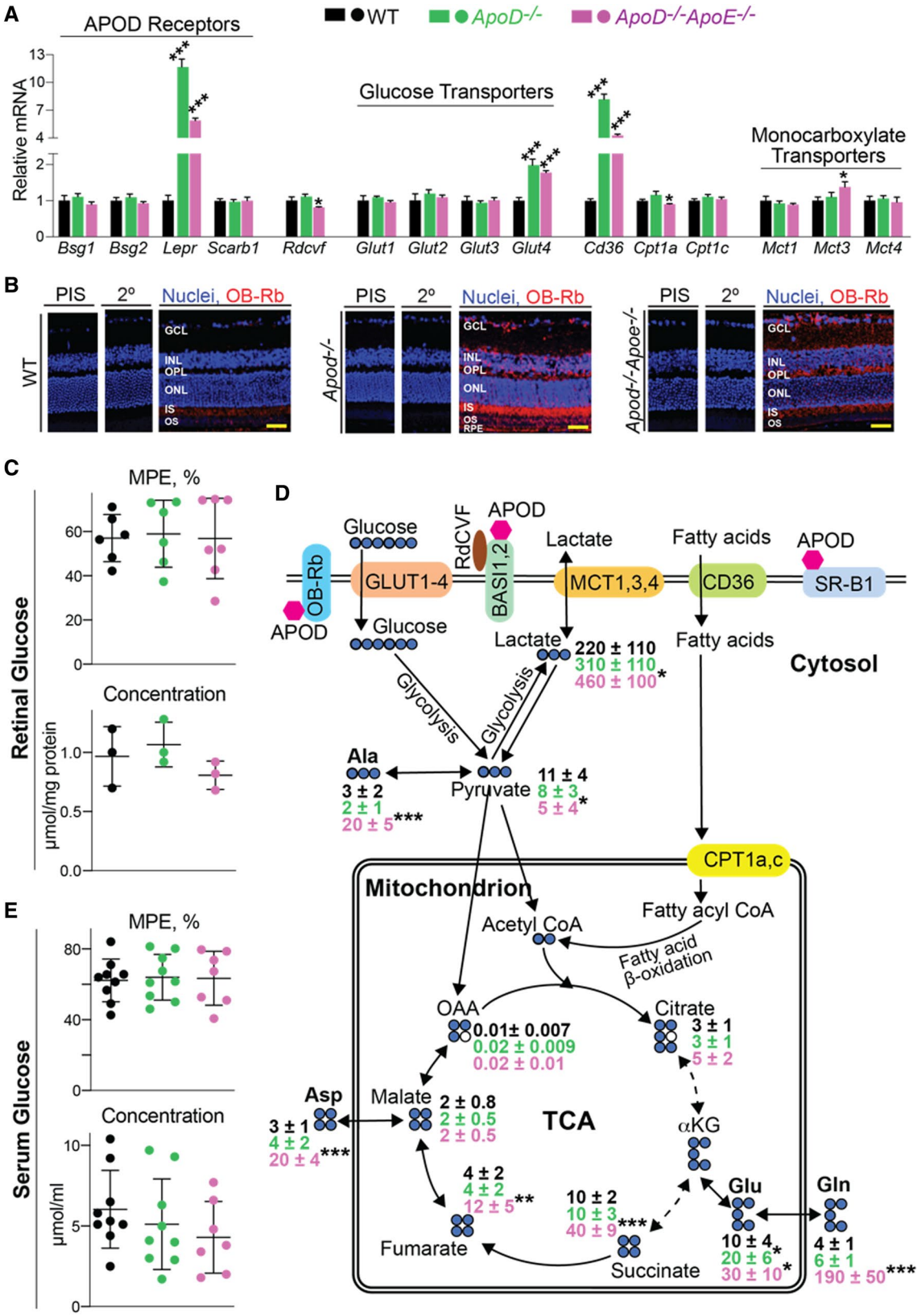
A
APOD Receptors
WT
ApoD-/-
ApoD-/-ApoE-/-
Relative mRNA
Glucose Transporters
Monocarboxylate Transporters
Bsg1 Bsg2 Lepr Scarb1 Rdcvf Glut1 Glut2 Glut3 Glut4 Cd36 Cpt1a Cpt1c Mct1 Mct3 Mct4
B
PIS 2° Nuclei, OB-Rb
WT
Apod-/-
Apod-/-Apoe-/-
GCL INL OPL ONL IS OS RPE
C
Retinal Glucose
MPE, %
Concentration
µmol/mg protein
D
Glucose GLUT1-4 RdCVF BASI1,2 APOD Lactate MCT1,3,4 Fatty acids CD36 APOD SR-B1 OB-Rb APOD
Cytosol
Glycolysis
Ala
Pyruvate
CPT1a,c
Mitochondrion
Acetyl CoA
Fatty acyl CoA
Fatty acid β-oxidation
OAA
Citrate
Asp
Malate
TCA
αKG
Glu
Gln
Fumarate
Succinate
E
Serum Glucose
MPE, %
Concentration
µmol/ml

◂**Fig. 6** Retinal glucose homeostasis. **a** Retinal gene expression. Results are mean ± SD of the triplicate measurements in pooled samples of the retinas from 5–7 wild type (WT, C57BL/6J), *ApoD*$^{-/-}$, and *ApoD*$^{-/-}$*ApoE*$^{-/-}$ mice; all mice were 6–8-month-old males. **b** Representative images ($n = 3$–4 mice/genotype) of OB-Rb immunolocalization in mouse retina. Nuclei are in blue (stained with DAPI), and immunoreactivity for OB-Rb is in red. PIS, preimmune serum, used as control stains. 2°, another control stain with secondary antibody. *GCL* ganglion cell layer, *INL* inner nuclear layer, *OPL* outer plexiform layer, *ONL* outer nuclear layer, *IS* photoreceptor inner segments, *OS* photoreceptor outer segments, *RPE* retinal pigment epithelium. *Scale bars* 50 µm. **c** and **e**, retinal and serum [U-^{13}C]glucose molar percent enrichment (MPE) and glucose concentrations, respectively. **d** Retinal glucose metabolism ($n = 7$–9/genotype). Blue circles represent ^{13}C-labeling of glucose (6 carbons) and subsequent ^{13}C incorporation into the intermediates of various metabolic pathways. Numbers next to each metabolite represent its absolute flux ($\times 10^{-3}$, nmol/mg of protein). *Ala* alanine, *Asp* aspartate, *Gln* glutamine, *Glu* glutamate, *αKG* α-ketoglutarate, *OAA* oxaloacetate, *TCA* the tricarboxylic acid cycle. **c**–**e** All results are means ± SD of the measurements in pooled samples of two retinas from individual mice. **a**, **c**–**e** The statistical significance was assessed by a two-tailed, unpaired Student's *t* test vs the WT retina; $*P \le 0.05$; $**P \le 0.01$; $***P \le 0.001$

The expression of *Glut1* and *Glut3* was unchanged in the *ApoD*$^{-/-}$ and *ApoD*$^{-/-}$*ApoE*$^{-/-}$ retinas, consistent with the proteomics data, which similarly documented the unaltered expression of these abundant transporters (Suppl. Tables S6, S7). The expression of *Glu2*, which was not detected by retinal proteomics, was unchanged as well, and only the expression of *Glut4*, the insulin-dependent glucose transporter, was upregulated in the *ApoD*$^{-/-}$ and *ApoD*$^{-/-}$*ApoE*$^{-/-}$ retinas, 2.0- and 1.8-fold, respectively (Fig. 6a). GLUT4 is stored intracellularly and translocates to the plasma membrane to enhance glucose uptake in response to stimulation with insulin [85], which also regulates the translocation to the plasma membrane of CD36 (cluster of differentiation 36), a scavenger receptor for multiple ligands including fatty acids and other lipids [86]. Hence, we quantified the expression of *Cd36* and in addition the expression of *Cpt1a* and *Cpt1c*, the two isoforms of carnitine palmitoyltransferase, which catalyzes an essential step in the mitochondrial uptake of long chain fatty acids and their subsequent β-oxidation in the mitochondria [87]. The *Cd36* expression was upregulated 8.2- and 4.3-fold in the *ApoD*$^{-/-}$ and *ApoD*$^{-/-}$*ApoE*$^{-/-}$ retinas, respectively, whereas that of *Cpt1a* and *Cpt1c* was not altered in the *ApoD*$^{-/-}$ retina and only slightly decreased (*Cpt1a*) in the *ApoD*$^{-/-}$*ApoE*$^{-/-}$ retina. Lastly, we measured the mRNA for *Mct1*, *Mct3*, and *Mct4*, the monocarboxylate transporters 1, 3, and 4, which flux lactate, the product of anaerobic glycolysis, in and outside cells. These measurements revealed no major changes in the expression of *Mct1*, *Mct3*, and *Mct4*, except a small increase in the *Mct3* levels in the *ApoD*$^{-/-}$*ApoE*$^{-/-}$ retina. Thus, both *ApoD*$^{-/-}$ and *ApoD*$^{-/-}$*ApoE*$^{-/-}$ retinas had an upregulation of *Lepr*, *Glut4*, and *Cd36*, the key players in glucose and fatty acid metabolism.

Glucose tolerance test

This test utilizes a blood sample and evaluates the insulin-dependent glucose disposal by the whole body. Mice of 6 and 12 months of age were assessed. At both time points, *ApoD*$^{-/-}$ mice had impaired glucose elimination either 60–120 min (at 6 months) or 90–150 min (at 12 months) post-glucose injection (Fig. 7). In addition, at 12 months, this genotype also had moderate (up to 20%) but a statistically significant increase in the fasting serum glucose levels as compared to wild type mice. Conversely, at both time points, glucose elimination was faster in *ApoD*$^{-/-}$*ApoE*$^{-/-}$ mice than in wild-type mice, and the fasting serum glucose levels were either normal (at 6 months) or decreased by 36% (at 12 months). Thus, depending on the background, C57BL/6J or *ApoE*$^{-/-}$, ablation of *ApoD* had opposite effects on the glucose elimination from the blood—decreasing in C57BL/6J mice and increasing in *ApoE*$^{-/-}$ mice. Importantly, these effects were observed at both 6 and 12 months of age.

Metabolic fluxes of retinal glucose in vivo

A novel approach was used, in which retinal glucose metabolism was measured 30 min post-intraperitoneal injection with the [U-^{13}C]glucose. The ^{13}C glucose enrichment was ~58% in the retina and ~63% in the serum (Fig. 6c, e) both in wild-type and knockout mice, an important result suggesting that retinal glucose is in the rapid and nearly complete (> 90%) equilibrium with the serum glucose. This result also indicates that our isotopic experiments were carried out under the precursor (glucose) steady-state conditions, essential for tracing metabolic pathways and determination of fractional and absolute synthesis rates of metabolite products. The glucose concentrations were unchanged in the retina of *ApoD*$^{-/-}$ mice and were slightly decreased in *ApoD*$^{-/-}$*ApoE*$^{-/-}$ mice (Fig. 6c, e). The latter, however, was non-significant due to inter-animal variability. Hence statistically, the retinal glucose levels were the same in wild-type mice and the knockout genotypes. In *ApoD*$^{-/-}$ mice, the retinal glucose fluxes in the glycolysis, the tricarboxylic acid cycle (TCA), and amino acid formation were essentially unchanged relative to wild-type mice (Fig. 6d), despite an apparent mitochondrial stress (Fig. 5e). Yet in *ApoD*$^{-/-}$*ApoE*$^{-/-}$ mice, the glycolytic glucose flux was increased as indicated by a decrease in the pyruvate concentrations and increase in the lactate concentrations, consistent with increased *Mct3* expression. The concentrations of citrate, succinate, and fumarate were increased as well indicating elevated flux through the TCA. The ^{13}C-labeling

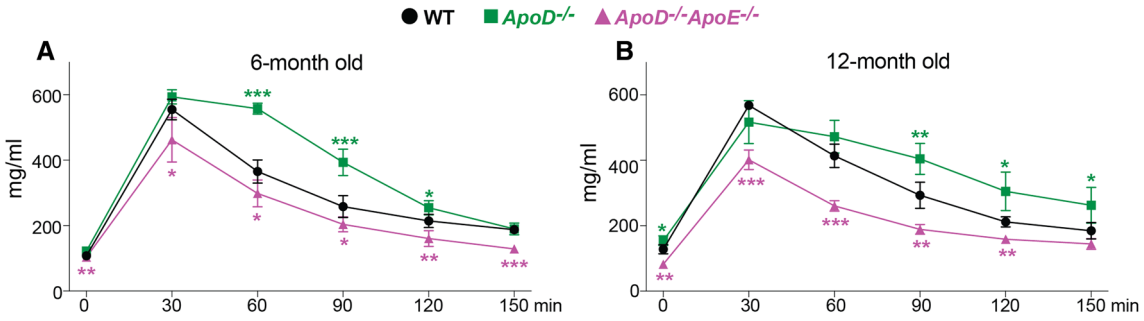

Fig. 7 Glucose tolerance test. Results are means ± SD of the measurements in blood samples from individual animals ($n = 5$–8/genotype/age group). The statistical significance was assessed by a two-way ANOVA followed by the Bonferroni correction; $^{*}P \leq 0.05$, $^{**}P \leq 0.01$, $^{***}P \leq 0.001$

also revealed a marked increase in the flux as well as concentrations of alanine, glutamine, glutamate, and aspartate from pyruvate, α-ketoglutarate, and oxaloacetate/malate, respectively. This increased flux in the cytosolic amino acids likely reflects increased mitochondrial cataplerosis rather than ATP production. Thus, the glucose metabolism was unchanged in the *ApoD*$^{-/-}$ retina and did not mirror that in the organs determining the blood glucose levels. In contrast, the glucose metabolism was enhanced in the *ApoD*$^{-/-}$*ApoE*$^{-/-}$ retina and mirrored that in the whole body.

Retinal effects of different diets

Increased *Lepr*, *Glut4*, and *Cd36* expression in *ApoD*$^{-/-}$ mice and involvement of the encoded proteins in fatty acid and glucose metabolism prompted two dietary studies. In the first, *ApoD*$^{-/-}$ mice were put for 5 months on Western diet containing 0.3% cholesterol and 0.21% fat. In the second, *ApoD*$^{-/-}$ mice were put for 3 months on HFHS diet containing 17% sucrose and 20.5% fat and also receiving 20% fructose in drinking water. Only the HFHS diet seemed to affect the retina of *ApoD*$^{-/-}$ mice (the data for Western diet are not shown) as the margins of some of the retinal capillaries in the outer retina became diffused on FA (Fig. 8a, b), suggestive of their increased permeability, a change characteristic of early stage diabetic retinopathy [88–90]. In addition, the leakage from some of the choroidal neovessels in mice, which had this abnormality, became more prominent as indicated by an increased hyperfluorescence on FA (Fig. 8a). Increased vasopermeability of mice on HFHS diet was further confirmed by staining for albumin, normally remaining restricted within blood vessels [91]. The anti-albumin staining was more prominent in *ApoD*$^{-/-}$ mice on HFHS diet than in wild type or *ApoD*$^{-/-}$ mice on regular diet (Fig. 8c) and also revealed the pathologic growth of some of the choriocapillaries toward the outer retina in *ApoD*$^{-/-}$ mice on HFHS diet. Thus, likely a combination of the dietary stress from the HFHS diet but not the Western diet and the *ApoD*$^{-/-}$ genotype that increased the permeability of chorioretinal blood vessels and enhanced pathologic choroidal neovascularization in the studied animals.

Discussion

The present study is a part of our on-going investigation of the role of different apolipoproteins in retinal structure, function, and cholesterol maintenance. Previously, we and others characterized in great detail *ApoE*$^{-/-}$ mice [6, 10, 92–97]. Herein, we conducted retinal evaluations of *ApoD*$^{-/-}$ and *ApoD*$^{-/-}$*ApoE*$^{-/-}$ mice. We found that the retinal sterol profile was not altered in *ApoD*$^{-/-}$ mice (Fig. 2) as is the retinal abundance of APOE or other major retinal apolipoprotein (APOA1, APOA2, APOA4, and APOJ, Suppl. Table S6). Reciprocally, the *ApoD* expression was not upregulated in the *ApoE*$^{-/-}$ retina and in fact was slightly decreased [6]. Thus, unlike the brain [54, 55], the expression of APOE and APOD does not seem to be coordinated in mouse retina (Fig. 2), and APOD does not appear to be a major contributor, at least under normal conditions (in C57BL/6J mice), to retinal cholesterol maintenance.

We generated *ApoD*$^{-/-}$*ApoE*$^{-/-}$ mice to ascertain whether APOD and APOE play redundant, complementary or opposing roles in the retina. However, our results suggest that neither of these roles is applicable to the APOD–APOE pair, and that the APOD–APOE interplay is more complex than originally thought. This complexity is exemplified by the unchanged cholesterol levels in the *ApoD*$^{-/-}$ retina and decreased cholesterol levels in the *ApoD*$^{-/-}$*ApoE*$^{-/-}$ retina as compared to the *ApoE*$^{-/-}$ retina (Fig. 2). Similarly, glucose metabolism was not changed in the *ApoD*$^{-/-}$ retina and enhanced in the *ApoD*$^{-/-}$*ApoE*$^{-/-}$ retina (Fig. 6d). Lastly, the IS mitochondrial morphology and retinal function seemed to be worse in *ApoD*$^{-/-}$ than *ApoD*$^{-/-}$*ApoE*$^{-/-}$ mice (Figs. 4, 5). Why do some of the effects of *ApoD* ablation depend on the background, C57BL/6J or *ApoE*$^{-/-}$? Previously, we

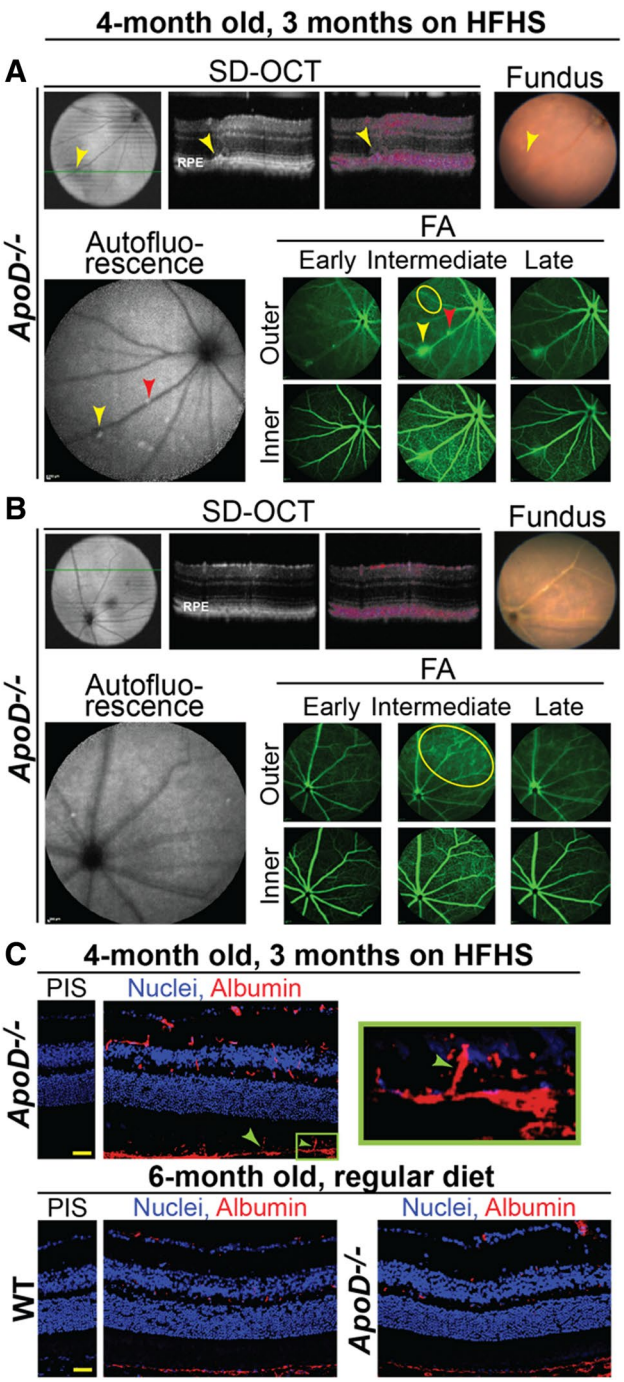

Fig. 8 Retinal in vivo imaging and immunohistochemistry of mice on high- fat high-sugar (HFHS) diet. **a**, **b** Representative ($n = 5$/genotype) assessments by spectral domain-optical coherence tomography (SD-OCT), fundus color imaging (Fundus), fundus autofluorescence (Autofluorescence), and fundus fluorescein angiography (FA) after an injection with sodium fluorescein. The SD-OCT panels show a fundus image and two retinal cross-sections (from left to right), the latter is a Doppler flow, which reflects the direction of the blood flow. The FA panels show an early, intermediate and late stage fundus fluorescence (from left to right) with the laser beam being focused either on the outer (Outer) or inner (Inner) retina. Yellow ovals outline some of the areas in the retina with increased permeability of the blood vessels. Yellow and magenta arrowheads point to the blood vessel leakage in different locations. No sex-based differences were detected, hence only images of male mice are shown. **c** Representative ($n = 3$-5/genotype) immunohistochemistry stains for albumin to assess vascular permeability. *PIS* preimmune serum, used as control stains. Nuclei are in blue (stained with DAPI), and immunoreactivity for albumin is in red. Green arrowheads point towards some of the choroidal neovessels growing toward the outer retina. Green rectangle in the upper left panel denotes the region shown at a higher magnification on the right. *Scale bars* 50 µm

found that *ApoE* ablation induces a number of compensatory responses in mouse retina, thus leading to a minor retinal phenotype of mice [6]. Herein, we found the changes in the gene and protein expression in the retina of *ApoD*$^{-/-}$ mice as well (Table 1, Suppl. Figs. S1, S3, S5). However, these changes did not seem to be sufficient to compensate for lack of APOD, thus leading to the retinal phenotype (Figs. 3, 4). Accordingly, full or partial rescue of this retinal phenotype in *ApoD*$^{-/-}$*ApoE*$^{-/-}$ mice was probably due to the compensatory responses elicited by lack of APOE and the interplay between the responses induced by lack of APOD and APOE. Remarkably, this interplay also increased the retinal glucose flux and cataplerosis as well as the whole-body glucose disposal (Figs. 6, 7).

Previously, APOE has been linked to leptin receptor by showing that the receptor expression levels in the brain of transgenic *ApoE4* and *ApoE3* mice vary and are determined by the human APOE isoform that these mice carry [98]. Herein, by studying the *ApoD*$^{-/-}$ and *ApoD*$^{-/-}$*ApoE*$^{-/-}$ retina, we linked APOD to leptin receptor, a novel finding. We showed for the first time that the retina not only expresses *Lepr* (Fig. 6a) but also its protein product (OB-Rb), which was localized to the IS (Fig. 6b), the site of APOD immunolocalization (Fig. 1). Moreover, we found that the expression of both *Lepr* and OB-Rb was increased in the *ApoD*$^{-/-}$ and *ApoD*$^{-/-}$*ApoE*$^{-/-}$ retinas as are the expression of *Glut4* and *Cd36*. Therefore, we suggest the APOD-OB-Rb-GLUT4/CD36 axis. This axis would be consistent with OB-Rb being the master regulator of glucose and fatty metabolism, studies documenting the leptin-induced expression of CD36, and knowledge that insulin receptor, which regulates GLUT4 translocation to plasma membranes, is expressed in the retina in several layers including the IS [99–102]. Retinal detection of OB-Rb is also in agreement with the recent discovery that in addition to glucose, the retina uses the fatty acid β-oxidation for energy production [103]. Hence, retinal OB-Rb identification reveals a mechanism of fatty acid delivery to the retina. Why is the OB-Rb expression increased in the *ApoD*$^{-/-}$ and *ApoD*$^{-/-}$*ApoE*$^{-/-}$ retina? This is not clear yet, however it was shown that APOD binds to the cytoplasmic portion of Ob-Rb but not Ob-Ra, the short form of the receptor [27]. It is conceivable that lack of APOD destabilizes Ob-Rb and leads to a compensatory upregulation of this receptor in the

retina. The APOD-Ob-Rb binding could be analogous to the APOD interaction with lecithin:cholesterol acyltransferase, when complex formation with APOD stabilizes and activates this enzyme [104]. Further research is needed to support this explanation.

Simultaneous upregulation of the retinal *Lepr* and *Glut4* expression, increase in retinal OB-Rb abundance (Fig. 6b), and changes in the whole-body glucose disposal in *ApoD*$^{-/-}$ and *ApoD*$^{-/-}$*ApoE*$^{-/-}$ mice (Fig. 7) gave impetus to unique in vivo studies utilizing the ^{13}C glucose injections (Fig. 6d). Typically, in vivo metabolic flux studies using stable isotope tracers involve primed infusion of the isotope over several hours to maintain the steady state of the ^{13}C-labeled precursor molecule across multiple compartments, i.e., between blood and tissue. Herein, we were able to measure the metabolomics fluxes following a single bolus of ^{13}C-labeled glucose. This novel, to the best of our knowledge, approach demonstrated a near full equilibration of ^{13}C-glucose in the blood and retina compartments and produced a measurable ^{13}C label incorporation into metabolites of several key metabolic pathways, i.e., retinal aerobic and anaerobic glycolysis, TCA, and amino acid formation. In addition, the steady state in vivo concentrations of different glucose metabolites were determined. Specifically, in the *ApoD*$^{-/-}$ retina, the steady-state glucose concentrations and subsequent glucose flux to different pathways remained unchanged (Fig. 6c, d), thus suggesting that the retinal glucose input was not changed as well. The latter could be because the major mechanism for glucose input to retinal cells is via GLUT1, GLUT2, and GLUT3, the facilitative glucose transporters [105], whose abundance in the retina is much higher than that of GLUT4 [106, 107]. Accordingly, either the *Glut4* upregulation in the *ApoD*$^{-/-}$ retina does not contribute significantly to this major mechanism or/and GLUT4 may not be delivered to the plasma membranes as suggested by retinal proteomics (Suppl. Fig. S3). As for the unchanged glucose output in the *ApoD*$^{-/-}$ retina despite the apparent mitochondrial stress (Fig. 5), this could be due to enhanced mitochondrial fission or fusion (Fig. 5), a protective response against mitochondrial stress and disfunction [82, 108]. Not only the mitochondria-rich photoreceptors but also other cell types contribute to glucose metabolism in the retina [109, 110].

In the *ApoD*$^{-/-}$*ApoE*$^{-/-}$ retina, the steady-state glucose concentrations were the same as in the wild-type retina, yet the glucose flux to different pathways was increased (Fig. 6d), thus suggesting that retinal glucose input was increased as well. This increased input could be the consequence of the *Glut4* upregulation and unimpaired GLUT4 delivery to plasma membranes. Increased glucose output could be a compensatory mechanism to an increased energy demand due to enhancement of vesicular trafficking (Suppl. Fig. S4). In any case, increased glucose flux through TCA may reflect a general mechanism whereby *ApoD*$^{-/-}$*ApoE*$^{-/-}$ mice have enhanced whole-body glucose disposal (Fig. 7). In addition, increased retinal glucose metabolism may contribute to partial restoration of the ERG amplitudes as compared to *ApoD*$^{-/-}$ mice as energy metabolism and neuronal activity are tightly coupled [105]. Similarly, increased glucose flux into the amino acid formation, including the synthesis of glutamate, the major neurotransmitter in the retina [111], could also contribute to enhanced retinal function of *ApoD*$^{-/-}$*ApoE*$^{-/-}$ mice as compared to *ApoD*$^{-/-}$ mice. A demand for increased amino acid formation could in turn be a compensatory response to a decreased expression of different crystallins, which are retinal chaperones [112]. Thus, *ApoE* ablation revealed context-specific APOD roles in glucose metabolism.

Our SD-OCT and FA characterizations suggested that lack of APOD affects the status of choroidal and retinal blood vessels as well as retinal function. Indeed, *ApoD*$^{-/-}$ mice had occasional choroidal neovascularization, and this neovascularization was exacerbated by a HFHS diet (Fig. 8a). In addition, HFHS diet led to an increase in permeability of retinal capillaries and choriocapillaries (Fig. 8a, b). Previously, the APOD upregulation was shown to suppress the PI3K-Akt-eNOS signaling and thereby angiogenesis of human umbilical vein endothelial cells [29]. Yet, in the case of retina, the proteomics analysis of *ApoD*$^{-/-}$ and *ApoD*$^{-/-}$*ApoE*$^{-/-}$ mice did not identify changes in the proteins from this signaling pathway. Rather a group of differentially expressed proteins participating in cellular adhesion (PDLI3, TLN2, E41L5, and TINAL in *ApoD*$^{-/-}$ mice) was identified (Table 1, Suppl. Fig. S1). Of them, a decreased abundance of TLN2 is worth consideration as TLN2 is a major component of focal adhesion plaques and was suggested to play a role in the RPE attachment to Bruch's membrane [113]. Accordingly, decreased levels of TLN2 could impair the RPE-Bruch's membrane adherence and thereby facilitate the protrusion through Bruch's membrane and RPE of the growing choroidal neovessels. In addition, the *ApoD*$^{-/-}$ retina had an increased expression of *Cd36*, a receptor involved in multiple biological processes including fatty acid transport, angiogenesis, and inflammation [86, 114]. In the latter, CD36 was suggested to be the master regulator of inflammasome activation in macrophages during atherosclerosis, Alzheimer's disease, and type 2 diabetes [114]. Chronic inflammation in diabetes contributes to damage of retinal microvasculature [88–90]. Hence, we hypothesize that increased permeability of retinal capillaries in *ApoD*$^{-/-}$ mice on HFHS diet (Fig. 8a, b) could be due in part to the upregulation of *Cd36*, which is localized in the microvascular endothelium and macrophages as well as both sides of the RPE [115–117]. Changes characteristic of early stage diabetic retinopathy in *ApoD*$^{-/-}$ mice on HFHS diet are also supported by increased expression of aquaporin

4 (AQ4, Table 1), the most abundant retinal water channel [118]. AQ4 is expressed in the Muller cell endfeet and perivascular space, and its retinal levels were shown to be increased in diabetic rats as a compensatory response [119, 120]. Thus, altered expression of TLN2, AQ4, and *Cd36* provides a mechanistic insight into vascular abnormalities in $ApoD^{-/-}$ mice on HFHS diet.

$ApoD^{-/-}$ mice had decreased amplitudes of all ERGs (Fig. 4) indicating impairments in retinal function. This could be due, at least in part, to changes in the levels RAB4B, PLST, and particularly CAC1A along with RIMS2 (Table 1, Suppl. Fig. S1). CAC1A is a subunit of voltage-dependent P/Q-type calcium channel and is known to participate in triggering the neurotransmitter release [121, 122]. RIMS2 is an essential component of the synaptic active zones (sites of exocytosis in synapses) and a regulator of synaptic vesicle exocytosis; this protein is abundant in photoreceptor ribbon synapses [123, 124]. Decreased abundance of CAC1 and RIMS2 could affect neurotransmission and thereby ERGs, which reflect electrical responses in the retina. Additional studies are required to better understand the role of TLN2, CAC1, and RIMS2 in the $ApoD^{-/-}$ retina.

In summary, by characterizing $ApoD^{-/-}$ and $ApoD^{-/-}ApoE^{-/-}$ mice, we assessed the retinal importance of APOD and the APOD–APOE interplay. In wild-type animals, APOD does not contribute significantly to retinal cholesterol and glucose homeostasis but is important for the normal status of chorioretinal vasculature and retinal function. In $ApoE^{-/-}$ mice, APOD is a negative and positive regulator of the retinal cholesterol levels and glucose utilization, respectively, and is of minor importance for chorioretinal vasculature and retinal function. In both backgrounds, APOD was linked to the leptin receptor OB-Rb, which was found to be expressed in the retina, and thereby to the GLUT4 transporter and CD36 receptor, important for glucose and fatty acid input, respectively. In vivo metabolic flux studies determined for the first time the steady state in vivo concentrations of different glucose metabolites and retinal glucose fluxes into glycolysis, TCA, and amino acid formation. The proteomics studies mapped the key proteins, whose altered abundance may underline the APOD effects on retinal choriovasculature (TLN2, AQ4, and CD36) and synaptic function (CAC1A and RIMS2). The APOD effects seem to be background specific and represent the interplay between the compensatory mechanism elicited by lack of APOD and APOE.

Acknowledgements This work was supported in part by NIH grants EY018383 and EY011373 (I.A.P.) and the unrestricted grant from Research to Prevent Blindness. Irina A. Pikuleva is a Carl F. Asseff Professor of Ophthalmology. The authors thank the Visual Sciences Research Center Core Facilities (supported by National Institutes of Health Grant P30 EY11373) for assistance with mouse breeding (Heather Butler and Kathryn Franke), animal genotyping (John Denker), tissue sectioning (Catherine Doller), and microscopy (Scott Howell and Anthony Gardella). We are also grateful to Dr. Hisashi Fujioka (Electron Microscopy Core facility) for help with studies of retinal ultrastructure, to Danie Schlatzer (Proteomics and Small Molecule Mass Spectrometry Core) for conducting retinal label free analysis, and to Dr. Neal Peachey for assistance with the ERG studies.

Author contributions IAP and AMP conception and study design; IAP study supervision; NED, NM, AMP, TD, AAA, AS, EP, ES, and IB produced and analyzed data; IAP, NM, AMP, and IB wrote and edited the manuscript.

Compliance with ethical standards

Conflict of interest The authors have no conflicts of interest to declare.

References

1. Fliesler SJ, Bretillon L (2010) The ins and outs of cholesterol in the vertebrate retina. J Lipid Res 51:3399–3413. https://doi.org/10.1194/jlr.R010538
2. Pikuleva IA, Curcio CA (2014) Cholesterol in the retina: the best is yet to come. Prog Retin Eye Res 41:64–89. https://doi.org/10.1016/j.preteyeres.2014.03.002
3. Tserentsoodol N, Gordiyenko NV, Pascual I et al (2006) Intraretinal lipid transport is dependent on high density lipoprotein-like particles and class b scavenger receptors. Mol Vis 12:1319–1333
4. Tserentsoodol N, Sztein J, Campos M et al (2006) Uptake of cholesterol by the retina occurs primarily via a low density lipoprotein receptor-mediated process. Mol Vis 12:1306–1318
5. Mahley RW (2016) Central nervous system lipoproteins: APOE and regulation of cholesterol metabolism. Arterioscler Thromb Vasc Biol 36:1305–1315. https://doi.org/10.1161/ATVBAHA.116.307023
6. Saadane A, Petrov A, Mast N et al (2018) Mechanisms that minimize retinal impact of apolipoprotein e absence. J Lipid Res 59:2368–2382. https://doi.org/10.1194/jlr.M090043
7. Chernick D, Ortiz-Valle S, Jeong A et al (2019) Peripheral versus central nervous system APOE in Alzheimer's disease: interplay across the blood-brain barrier. Neurosci Lett 708:134306. https://doi.org/10.1016/j.neulet.2019.134306
8. Kim J, Basak JM, Holtzman DM (2009) The role of apolipoprotein e in Alzheimer's disease. Neuron 63:287–303. https://doi.org/10.1016/j.neuron.2009.06.026
9. Zhao N, Liu CC, Qiao W et al (2018) Apolipoprotein e, receptors, and modulation of Alzheimer's disease. Biol Psychiatry 83:347–357. https://doi.org/10.1016/j.biopsych.2017.03.003
10. Levy O, Lavalette S, Hu SJ et al (2015) APOE isoforms control pathogenic subretinal inflammation in age-related macular degeneration. J Neurosci 35:13568–13576. https://doi.org/10.1523/jneurosci.2468-15.2015
11. Mayeux R, Stern Y, Ottman R et al (1993) The apolipoprotein epsilon 4 allele in patients with Alzheimer's disease. Ann Neurol 34:752–754. https://doi.org/10.1002/ana.410340527
12. Corder EH, Saunders AM, Strittmatter WJ et al (1993) Gene dose of apolipoprotein e type 4 allele and the risk of Alzheimer's disease in late onset families. Science 261:921–923
13. Corder EH, Saunders AM, Risch NJ et al (1994) Protective effect of apolipoprotein e type 2 allele for late onset Alzheimer disease. Nat Genet 7:180–184. https://doi.org/10.1038/ng0694-180
14. Klaver CC, Kliffen M, van Duijn CM et al (1998) Genetic association of apolipoprotein e with age-related macular degeneration. Am J Hum Genet 63:200–206

15. Souied EH, Benlian P, Amouyel P et al (1998) The epsilon4 allele of the apolipoprotein e gene as a potential protective factor for exudative age-related macular degeneration. Am J Ophthalmol 125:353–359
16. McKay GJ, Patterson CC, Chakravarthy U et al (2011) Evidence of association of APOE with age-related macular degeneration: a pooled analysis of 15 studies. Hum Mutat 32:1407–1416. https://doi.org/10.1002/humu.21577
17. Mak AC, Pullinger CR, Tang LF et al (2014) Effects of the absence of apolipoprotein e on lipoproteins, neurocognitive function, and retinal function. JAMA Neurol 71:1228–1236. https://doi.org/10.1001/jamaneurol.2014.2011
18. Elliott DA, Weickert CS, Garner B (2010) Apolipoproteins in the brain: implications for neurological and psychiatric disorders. Clin Lipidol 51:555–573. https://doi.org/10.2217/CLP.10.37
19. Drayna D, Fielding C, McLean J et al (1986) Cloning and expression of human apolipoprotein D cDNA. J Biol Chem 261:16535–16539
20. McConathy WJ, Alaupovic P (1973) Isolation and partial characterization of apolipoprotein D: a new protein moiety of the human plasma lipoprotein system. FEBS Lett 37:178–182. https://doi.org/10.1016/0014-5793(73)80453-3
21. Perdomo G, Kim DH, Zhang T et al (2010) A role of apolipoprotein d in triglyceride metabolism. J Lipid Res 51:1298–1311. https://doi.org/10.1194/jlr.M001206
22. Rassart E, Bedirian A, Do Carmo S et al (2000) Apolipoprotein D. Biochim Biophys Acta 1482:185–198
23. Soiland H, Soreide K, Janssen EA et al (2007) Emerging concepts of apolipoprotein D with possible implications for breast cancer. Cell Oncol 29:195–209
24. Chen YW, Gregory CM, Scarborough MT et al (2007) Transcriptional pathways associated with skeletal muscle disuse atrophy in humans. Physiol Genomics 31:510–520. https://doi.org/10.1152/physiolgenomics.00115.2006
25. Dassati S, Waldner A, Schweigreiter R (2014) Apolipoprotein D takes center stage in the stress response of the aging and degenerative brain. Neurobiol Aging 35:1632–1642. https://doi.org/10.1016/j.neurobiolaging.2014.01.148
26. Eichinger A, Nasreen A, Kim HJ et al (2007) Structural insight into the dual ligand specificity and mode of high density lipoprotein association of apolipoprotein D. J Biol Chem 282:31068–31075. https://doi.org/10.1074/jbc.M703552200
27. Liu Z, Chang GQ, Leibowitz SF (2001) Apolipoprotein D interacts with the long-form leptin receptor: a hypothalamic function in the control of energy homeostasis. FASEB J 15:1329–1331. https://doi.org/10.1096/fj.00-0530fje
28. Najyb O, Brissette L, Rassart E (2015) Apolipoprotein D internalization is a basigin-dependent mechanism. J Biol Chem 290:16077–16087. https://doi.org/10.1074/jbc.M115.644302
29. Lai CJ, Cheng HC, Lin CY et al (2017) Activation of liver x receptor suppresses angiogenesis via induction of ApoD. FASEB J. https://doi.org/10.1096/fj.201700374R
30. Sarjeant JM, Lawrie A, Kinnear C et al (2003) Apolipoprotein D inhibits platelet-derived growth factor-bb-induced vascular smooth muscle cell proliferated by preventing translocation of phosphorylated extracellular signal regulated kinase 1/2 to the nucleus. Arterioscler Thromb Vasc Biol 23:2172–2177. https://doi.org/10.1161/01.ATV.0000100404.05459.39
31. D'Souza AM, Neumann UH, Glavas MM et al (2017) The glucoregulatory actions of leptin. Mol Metab 6:1052–1065. https://doi.org/10.1016/j.molmet.2017.04.011
32. Banks AS, Davis SM, Bates SH et al (2000) Activation of downstream signals by the long form of the leptin receptor. J Biol Chem 275:14563–14572. https://doi.org/10.1074/jbc.275.19.14563
33. Bahrenberg G, Behrmann I, Barthel A et al (2002) Identification of the critical sequence elements in the cytoplasmic domain of leptin receptor isoforms required for janus kinase/signal transducer and activator of transcription activation by receptor heterodimers. Mol Endocrinol 16:859–872. https://doi.org/10.1210/mend.16.4.0800
34. Hileman SM, Pierroz DD, Masuzaki H et al (2002) Characterization of short isoforms of the leptin receptor in rat cerebral microvessels and of brain uptake of leptin in mouse models of obesity. Endocrinology 143:775–783. https://doi.org/10.1210/endo.143.3.8669
35. Blanco-Vaca F, Via DP, Yang CY et al (1992) Characterization of disulfide-linked heterodimers containing apolipoprotein d in human plasma lipoproteins. J Lipid Res 33:1785–1796
36. Tsukamoto K, Mani DR, Shi J et al (2013) Identification of apolipoprotein d as a cardioprotective gene using a mouse model of lethal atherosclerotic coronary artery disease. Proc Natl Acad Sci USA 110:17023–17028. https://doi.org/10.1073/pnas.1315986110
37. Ganfornina MD, Do Carmo S, Lora JM et al (2008) Apolipoprotein D is involved in the mechanisms regulating protection from oxidative stress. Aging Cell 7:506–515. https://doi.org/10.1111/j.1474-9726.2008.00395.x
38. Balbin M, Freije JM, Fueyo A et al (1990) Apolipoprotein D is the major protein component in cyst fluid from women with human breast gross cystic disease. Biochem J 271:803–807. https://doi.org/10.1042/bj2710803
39. Alvarez ML, Barbon JJ, Gonzalez LO et al (2003) Apolipoprotein D expression in retinoblastoma. Ophthalmic Res 35:111–116. https://doi.org/10.1159/000069130
40. Hunter S, Weiss S, Ou CY et al (2005) Apolipoprotein D is down-regulated during malignant transformation of neurofibromas. Hum Pathol 36:987–993. https://doi.org/10.1016/j.humpath.2005.06.018
41. Jin D, El-Tanani M, Campbell FC (2006) Identification of apolipoprotein D as a novel inhibitor of osteopontin-induced neoplastic transformation. Int J Oncol 29:1591–1599
42. Sasaki Y, Negishi H, Koyama R et al (2009) P53 family members regulate the expression of the apolipoprotein D gene. J Biol Chem 284:872–883. https://doi.org/10.1074/jbc.M807185200
43. Martineau C, Najyb O, Signor C et al (2016) Apolipoprotein D deficiency is associated to high bone turnover, low bone mass and impaired osteoblastic function in aged female mice. Metabolism 65:1247–1258. https://doi.org/10.1016/j.metabol.2016.05.007
44. Hitman GA, McCarthy MI, Mohan V et al (1992) The genetics of non-insulin-dependent diabetes mellitus in south india: an overview. Ann Med 24:491–497. https://doi.org/10.3109/07853899209167001
45. Vijayaraghavan S, Hitman GA, Kopelman PG (1994) Apolipoprotein-D polymorphism: a genetic marker for obesity and hyperinsulinemia. J Clin Endocrinol Metab 79:568–570. https://doi.org/10.1210/jcem.79.2.7913935
46. Baker WA, Hitman GA, Hawrami K et al (1994) Apolipoprotein D gene polymorphism: a new genetic marker for type 2 diabetic subjects in Nauru and South India. Diabet Med 11:947–952. https://doi.org/10.1111/j.1464-5491.1994.tb00252.x
47. Desai PP, Bunker CH, Ukoli FA et al (2002) Genetic variation in the apolipoprotein D gene among african blacks and its significance in lipid metabolism. Atherosclerosis 163:329–338. https://doi.org/10.1016/s0021-9150(02)00012-6
48. Desai PP, Hendrie HC, Evans RM et al (2003) Genetic variation in apolipoprotein D affects the risk of Alzheimer disease in African-Americans. Am J Med Genet B Neuropsychiatr Genet 116B:98–101. https://doi.org/10.1002/ajmg.b.10798

49. Helisalmi S, Hiltunen M, Vepsalainen S et al (2004) Genetic variation in apolipoprotein D and Alzheimer's disease. J Neurol 251:951–957. https://doi.org/10.1007/s00415-004-0470-8
50. Waldner A, Dassati S, Redl B et al (2018) Apolipoprotein D concentration in human plasma during aging and in Parkinson's disease: a cross-sectional study. Parkinsons Dis 2018:3751516. https://doi.org/10.1155/2018/3751516
51. Loerch PM, Lu T, Dakin KA et al (2008) Evolution of the aging brain transcriptome and synaptic regulation. PLoS ONE 3:e3329. https://doi.org/10.1371/journal.pone.0003329
52. de Magalhaes JP, Curado J, Church GM (2009) Meta-analysis of age-related gene expression profiles identifies common signatures of aging. Bioinformatics 25:875–881. https://doi.org/10.1093/bioinformatics/btp073
53. Lee CK, Weindruch R, Prolla TA (2000) Gene-expression profile of the ageing brain in mice. Nat Genet 25:294–297. https://doi.org/10.1038/77046
54. Terrisse L, Seguin D, Bertrand P et al (1999) Modulation of apolipoprotein D and apolipoprotein E expression in rat hippocampus after entorhinal cortex lesion. Brain Res Mol Brain Res 70:26–35
55. Jansen PJ, Lutjohann D, Thelen KM et al (2009) Absence of ApoE upregulates murine brain ApoD and ABCA1 levels, but does not affect brain sterol levels, while human ApoE3 and human ApoE4 upregulate brain cholesterol precursor levels. J Alzheimers Dis 18:319–329. https://doi.org/10.3233/JAD-2009-1150
56. Levros LC Jr, Labrie M, Charfi C et al (2013) Binding and repressive activities of apolipoprotein E3 and E4 isoforms on the human ApoD promoter. Mol Neurobiol 48:669–680. https://doi.org/10.1007/s12035-013-8456-0
57. Liu L, MacKenzie KR, Putluri N et al (2017) The glia-neuron lactate shuttle and elevated ROS promote lipid synthesis in neurons and lipid droplet accumulation in glia via APOE/D. Cell Metab 26(719–737):e716. https://doi.org/10.1016/j.cmet.2017.08.024
58. Kalaany NY, Mangelsdorf DJ (2006) LXRs and FXR: the yin and yang of cholesterol and fat metabolism. Annu Rev Physiol 68:159–191. https://doi.org/10.1146/annurev.physiol.68.033104.152158
59. Boyles JK, Notterpek LM, Anderson LJ (1990) Accumulation of apolipoproteins in the regenerating and remyelinating mammalian peripheral nerve. Identification of apolipoprotein D, apolipoprotein A-IV, apolipoprotein E, and apolipoprotein A-I. J Biol Chem 265:17805–17815
60. Montpied P, de Bock F, Lerner-Natoli M et al (1999) Hippocampal alterations of apolipoprotein E and D mRNA levels in vivo and in vitro following kainate excitotoxicity. Epilepsy Res 35:135–146. https://doi.org/10.1016/s0920-1211(99)00003-0
61. Kosacka J, Gericke M, Nowicki M et al (2009) Apolipoproteins D and E3 exert neurotrophic and synaptogenic effects in dorsal root ganglion cell cultures. Neuroscience 162:282–291. https://doi.org/10.1016/j.neuroscience.2009.04.073
62. Do Carmo S, Seguin D, Milne R et al (2002) Modulation of apolipoprotein D and apolipoprotein E mRNA expression by growth arrest and identification of key elements in the promoter. J Biol Chem 277:5514–5523. https://doi.org/10.1074/jbc.M105057200
63. Schafer NF, Luhmann UF, Feil S et al (2009) Differential gene expression in Ndph-knockout mice in retinal development. Investig Ophthalmol Vis Sci 50:906–916. https://doi.org/10.1167/iovs.08-1731
64. Zheng W, Mast N, Saadane A et al (2015) Pathways of cholesterol homeostasis in mouse retina responsive to dietary and pharmacologic treatments. J Lipid Res 56:81–97. https://doi.org/10.1194/jlr.M053439
65. Omarova S, Charvet CD, Reem RE et al (2012) Abnormal vascularization in mouse retina with dysregulated retinal cholesterol homeostasis. J Clin Investig 122:3012–3023. https://doi.org/10.1172/JCI63816
66. Saadane A, Mast N, Charvet CD et al (2014) Retinal and nonocular abnormalities in Cyp27a1(−/−)Cyp46a1(−/−) mice with dysfunctional metabolism of cholesterol. Am J Pathol 184:2403–2419. https://doi.org/10.1016/j.ajpath.2014.05.024
67. Curcio CA, Rudolf M, Wang L (2009) Histochemistry and lipid profiling combine for insights into aging and age-related maculopathy. Methods Mol Biol 580:267–281. https://doi.org/10.1007/978-1-60761-325-1_15
68. Zheng W, Reem RE, Omarova S et al (2012) Spatial distribution of the pathways of cholesterol homeostasis in human retina. PLoS ONE 7:e37926. https://doi.org/10.1371/journal.pone.0037926
69. Saadane A, Mast N, Trichonas G et al (2019) Retinal vascular abnormalities and microglia activation in mice with deficiency in cytochrome p450 46a1-mediated cholesterol removal. Am J Pathol 189:405–425. https://doi.org/10.1016/j.ajpath.2018.10.013
70. Mast N, Reem R, Bederman I et al (2011) Cholestenoic acid is an important elimination product of cholesterol in the retina: comparison of retinal cholesterol metabolism with that in the brain. Investig Ophthalmol Vis Sci 52:594–603. https://doi.org/10.1167/iovs.10-6021
71. Mast N, Shafaati M, Zaman W et al (2010) Marked variability in hepatic expression of cytochromes CYP7A1 and CYP27A1 as compared to cerebral CYP46A1. Lessons from a dietary study with omega 3 fatty acids in hamsters. Biochim Biophys Acta 1801:674–681. https://doi.org/10.1016/j.bbalip.2010.03.005
72. Pfaffl MW (2001) A new mathematical model for relative quantification in real-time RT-PCR. Nucleic Acids Res 29:e45
73. Zhang J, Xin L, Shan B et al (2012) Peaks DB: de novo sequencing assisted database search for sensitive and accurate peptide identification. Mol Cell Proteomics 11(M111):010587. https://doi.org/10.1074/mcp.M111.010587
74. Karnovsky MJ (1965) A formaldehyde-glutaraldehyde fixative of high osmolarity for use electron microscopy. J Cell Biol 27:137A
75. van Dijk TH, van der Sluijs FH, Wiegman CH et al (2001) Acute inhibition of hepatic glucose-6-phosphatase does not affect gluconeogenesis but directs gluconeogenic flux toward glycogen in fasted rats. A pharmacological study with the chlorogenic acid derivative S4048. J Biol Chem 276:25727–25735. https://doi.org/10.1074/jbc.M101223200
76. Pfrieger FW, Ungerer N (2011) Cholesterol metabolism in neurons and astrocytes. Prog Lipid Res 50:357–371. https://doi.org/10.1016/j.plipres.2011.06.002
77. Mast N, Bederman IR, Pikuleva IA (2018) Retinal cholesterol content is reduced in simvastatin-treated mice due to inhibited local biosynthesis albeit increased uptake of serum cholesterol. Drug Metab Dispos 46:1528–1537. https://doi.org/10.1124/dmd.118.083345
78. Castanho MA, Coutinho A, Prieto MJ (1992) Absorption and fluorescence spectra of polyene antibiotics in the presence of cholesterol. J Biol Chem 267:204–209
79. Coscas F, Coscas G, Souied E et al (2007) Optical coherence tomography identification of occult choroidal neovascularization in age-related macular degeneration. Am J Ophthalmol 144:592–599. https://doi.org/10.1016/j.ajo.2007.06.014
80. Robson JG, Frishman LJ (2014) The rod-driven a-wave of the dark-adapted mammalian electroretinogram. Prog Retin Eye Res 39:1–22. https://doi.org/10.1016/j.preteyeres.2013.12.003
81. Petrov AM, Astafev AA, Mast N et al (2019) The interplay between retinal pathways of cholesterol output and its effects on mouse retina. Biomolecules. https://doi.org/10.3390/biom9120867

82. Westermann B (2010) Mitochondrial fusion and fission in cell life and death. Nat Rev Mol Cell Biol 11:872–884. https://doi.org/10.1038/nrm3013
83. Hsieh WT, Hsu CJ, Capraro BR et al (2012) Curvature sorting of peripheral proteins on solid-supported wavy membranes. Langmuir 28:12838–12843. https://doi.org/10.1021/la302205b
84. Ait-Ali N, Fridlich R, Millet-Puel G et al (2015) Rod-derived cone viability factor promotes cone survival by stimulating aerobic glycolysis. Cell 161:817–832. https://doi.org/10.1016/j.cell.2015.03.023
85. Steinbusch LK, Schwenk RW, Ouwens DM et al (2011) Subcellular trafficking of the substrate transporters GLUT4 and CD36 in cardiomyocytes. Cell Mol Life Sci 68:2525–2538. https://doi.org/10.1007/s00018-011-0690-x
86. Febbraio M, Hajjar DP, Silverstein RL (2001) CD36: a class B scavenger receptor involved in angiogenesis, atherosclerosis, inflammation, and lipid metabolism. J Clin Investig 108:785–791. https://doi.org/10.1172/jci14006
87. Kerner J, Hoppel C (2000) Fatty acid import into mitochondria. Biochim Biophys Acta 1486:1–17. https://doi.org/10.1016/s1388-1981(00)00044-5
88. Tang J, Kern TS (2011) Inflammation in diabetic retinopathy. Prog Retin Eye Res 30:343–358. https://doi.org/10.1016/j.preteyeres.2011.05.002
89. Durham JT, Herman IM (2011) Microvascular modifications in diabetic retinopathy. Curr Diab Rep 11:253–264. https://doi.org/10.1007/s11892-011-0204-0
90. Stitt AW, Lois N, Medina RJ et al (2013) Advances in our understanding of diabetic retinopathy. Clin Sci (Lond) 125:1–17. https://doi.org/10.1042/CS20120588
91. Radu M, Chernoff J (2013) An in vivo assay to test blood vessel permeability. J Vis Exp. https://doi.org/10.3791/50062
92. Ong JM, Zorapapel NC, Rich KA et al (2001) Effects of cholesterol and apolipoprotein E on retinal abnormalities in ApoE-deficient mice. Investig Ophthalmol Vis Sci 42:1891–1900
93. Ong JM, Zorapapel NC, Aoki AM et al (2003) Impaired electroretinogram (ERG) response in apolipoprotein E-deficient mice. Curr Eye Res 27:15–24
94. Dithmar S, Curcio CA, Le NA et al (2000) Ultrastructural changes in Bruch's membrane of apolipoprotein E-deficient mice. Investig Ophthalmol Vis Sci 41:2035–2042
95. Kliffen M, Lutgens E, Daemen MJ et al (2000) The APO(*) E3-leiden mouse as an animal model for basal laminar deposit. Br J Ophthalmol 84:1415–1419
96. Malek G, Johnson LV, Mace BE et al (2005) Apolipoprotein E allele-dependent pathogenesis: a model for age-related retinal degeneration. Proc Natl Acad Sci USA 102:11900–11905. https://doi.org/10.1073/pnas.0503015102
97. Levy O, Calippe B, Lavalette S et al (2015) Apolipoprotein E promotes subretinal mononuclear phagocyte survival and chronic inflammation in age-related macular degeneration. EMBO Mol Med 7:211–226. https://doi.org/10.15252/emmm.201404524
98. Maioli S, Lodeiro M, Merino-Serrais P et al (2015) Alterations in brain leptin signalling in spite of unchanged CSF leptin levels in Alzheimer's disease. Aging Cell 14:122–129. https://doi.org/10.1111/acel.12281
99. Konstantinidis D, Paletas K, Koliakos G et al (2009) Signaling components involved in leptin-induced amplification of the atherosclerosis-related properties of human monocytes. J Vasc Res 46:199–208. https://doi.org/10.1159/000161234
100. Wang JL, Chinookoswong N, Scully S et al (1999) Differential effects of leptin in regulation of tissue glucose utilization in vivo. Endocrinology 140:2117–2124. https://doi.org/10.1210/endo.140.5.6681
101. Sanchez-Chavez G, Pena-Rangel MT, Riesgo-Escovar JR et al (2012) Insulin stimulated-glucose transporter glut 4 is expressed in the retina. PLoS ONE 7:e52959. https://doi.org/10.1371/journal.pone.0052959
102. Naeser P (1997) Insulin receptors in human ocular tissues. Immunohistochemical demonstration in normal and diabetic eyes. Ups J Med Sci 102:35–40. https://doi.org/10.3109/03009739709178930
103. Joyal JS, Sun Y, Gantner ML et al (2016) Retinal lipid and glucose metabolism dictates angiogenesis through the lipid sensor Ffar1. Nat Med 22:439–445. https://doi.org/10.1038/nm.4059
104. Fielding PE, Fielding CJ (1980) A cholesteryl ester transfer complex in human plasma. Proc Natl Acad Sci USA 77:3327–3330. https://doi.org/10.1073/pnas.77.6.3327
105. Wong-Riley MT (2010) Energy metabolism of the visual system. Eye Brain 2:99–116. https://doi.org/10.2147/EB.S9078
106. Mantych GJ, Hageman GS, Devaskar SU (1993) Characterization of glucose transporter isoforms in the adult and developing human eye. Endocrinology 133:600–607. https://doi.org/10.1210/endo.133.2.8344201
107. Watanabe T, Mio Y, Hoshino FB et al (1994) Glut2 expression in the rat retina: localization at the apical ends of muller cells. Brain Res 655:128–134. https://doi.org/10.1016/0006-8993(94)91606-3
108. Kam JH, Jeffery G (2015) To unite or divide: mitochondrial dynamics in the murine outer retina that preceded age related photoreceptor loss. Oncotarget 6:26690–26701. https://doi.org/10.18632/oncotarget.5614
109. Poitry-Yamate CL, Poitry S, Tsacopoulos M (1995) Lactate released by muller glial cells is metabolized by photoreceptors from mammalian retina. J Neurosci 15:5179–5191
110. Winkler BS, Arnold MJ, Brassell MA et al (1997) Glucose dependence of glycolysis, hexose monophosphate shunt activity, energy status, and the polyol pathway in retinas isolated from normal (nondiabetic) rats. Investig Ophthalmol Vis Sci 38:62–71
111. Bringmann A, Grosche A, Pannicke T et al (2013) GABA and glutamate uptake and metabolism in retinal glial (muller) cells. Front Endocrinol (Lausanne) 4:48. https://doi.org/10.3389/fendo.2013.00048
112. Thanos S, Bohm MR, Meyer zu Horste M et al (2014) Role of crystallins in ocular neuroprotection and axonal regeneration. Prog Retin Eye Res 42:145–161. https://doi.org/10.1016/j.preteyeres.2014.06.004
113. Philp NJ, Yoon MY, Hock RS (1990) Identification and localization of talin in chick retinal pigment epithelial cells. Exp Eye Res 51:191–198
114. Sheedy FJ, Grebe A, Rayner KJ et al (2013) CD36 coordinates NLRP3 inflammasome activation by facilitating intracellular nucleation of soluble ligands into particulate ligands in sterile inflammation. Nat Immunol 14:812–820. https://doi.org/10.1038/ni.2639
115. Ryeom SW, Silverstein RL, Scotto A et al (1996) Binding of anionic phospholipids to retinal pigment epithelium may be mediated by the scavenger receptor CD36. J Biol Chem 271:20536–20539
116. Houssier M, Raoul W, Lavalette S et al (2008) CD36 deficiency leads to choroidal involution via COX2 down-regulation in rodents. PLoS Med 5:e39. https://doi.org/10.1371/journal.pmed.0050039
117. Picard E, Houssier M, Bujold K et al (2010) CD36 plays an important role in the clearance of oxLDL and associated age-dependent sub-retinal deposits. Aging (Albany NY) 2:981–989. https://doi.org/10.18632/aging.100218
118. Nagelhus EA, Veruki ML, Torp R et al (1998) Aquaporin-4 water channel protein in the rat retina and optic nerve: polarized expression in muller cells and fibrous astrocytes. J Neurosci 18:2506–2519

119. Kumar B, Gupta SK, Srinivasan BP et al (2013) Hesperetin rescues retinal oxidative stress, neuroinflammation and apoptosis in diabetic rats. Microvasc Res 87:65–74. https://doi.org/10.1016/j.mvr.2013.01.002
120. Kumar B, Gupta SK, Nag TC et al (2014) Retinal neuroprotective effects of quercetin in streptozotocin-induced diabetic rats. Exp Eye Res 125:193–202. https://doi.org/10.1016/j.exer.2014.06.009
121. Xu HP, Zhao JW, Yang XL (2002) Expression of voltage-dependent calcium channel subunits in the rat retina. Neurosci Lett 329:297–300. https://doi.org/10.1016/s0304-3940(02)00688-2
122. Nimmrich V, Gross G (2012) P/Q-type calcium channel modulators. Br J Pharmacol 167:741–759. https://doi.org/10.1111/j.1476-5381.2012.02069.x
123. Lohner M, Babai N, Muller T et al (2017) Analysis of rim expression and function at mouse photoreceptor ribbon synapses. J Neurosci 37:7848–7863. https://doi.org/10.1523/JNEUROSCI.2795-16.2017
124. Grabner CP, Gandini MA, Rehak R et al (2015) RIM1/2-mediated facilitation of Cav1.4 channel opening is required for Ca^{2+}-stimulated release in mouse rod photoreceptors. J Neurosci 35:13133–13147. https://doi.org/10.1523/JNEUROSCI.0658-15.2015